We are IntechOpen,
the world's leading publisher of
Open Access books
Built by scientists, for scientists

5,600
Open access books available

137,000
International authors and editors

170M
Downloads

154
Countries delivered to

Our authors are among the

TOP 1%
most cited scientists

12.2%
Contributors from top 500 universities

CLARIVATE ANALYTICS

BOOK CITATION INDEX

INDEXED

WEB OF SCIENCE™

Selection of our books indexed in the Book Citation Index
in Web of Science™ Core Collection (BKCI)

Interested in publishing with us?
Contact book.department@intechopen.com

Numbers displayed above are based on latest data collected.
For more information visit www.intechopen.com

Chapter

A Novel Energy Management Control technique for PV-Battery System in DC Microgrids

Hadis Hajebrahimi, Sajjad Makhdoomi Kaviri,
Suzan Eren and Alireza Bakhshai

Abstract

This paper presents a new energy management control technique for PV-Battery system used in DC microgrids. The proposed control technique is performed based on a droop control algorithm that maintains DC-bus voltage in a desirable and required range adaptively. Tightly Regulating the bus voltage In the islanded mode of operation is very challenging. However, the proposed control method by introducing a nonlinear droop profile with four adaptive parameters shows its superiority. Adaptive parameters determined by the non-linear optimal algorithms. Tightly regulating the DC bus voltage during extensive changes in demand loads/sources within a DC Micro Grid is the responsibility of the adaptive parameters. Stability of the proposed method in the whole system for a very broad range of operating conditions are proved. Simulation results along with the experimental results verify the feasibility of the proposed approach while demonstrate its superior performance compared to the conventional control method.

Keywords: Adaptive Droop Control, PV-Battery Systems, DC Micro-grid Systems, Nonlinear Optimization, Renewable energy

1. Introduction

The main interfaces utilized in microgrids (MGs) for Renewable Energy Sources (RESs) and Energy Storage Systems (ESSs) are power electronic converters [1, 2]. MGs' reliable operation depends on these power electronic converters [3–6]. Specifically, power converters' control systems which introduced recently, can make MG systems more reliable for future mainstream power generation.

The AC power system are more common due to its advantages for long distance power transmission (i.e., transformers can be used to adjust optimal voltage levels). Thus, the development of micro-grid technology has been mostly confined to AC micro-grids [4, 5]. However, as the number of local micro-grids increase the need for long distance power transmission will significantly decline. Therefore, local DC micro-grids can potentially be more efficient due to the fact that many loads require DC power (e.g., electronic loads, LED lighting systems, electric vehicle charging, etc.). In addition, most renewable energy systems and energy storage systems are either inherently DC (batteries, solar panels) or incorporate a DC stage (inverter connected wind turbines) [6]. Since the number of DC sources and loads will
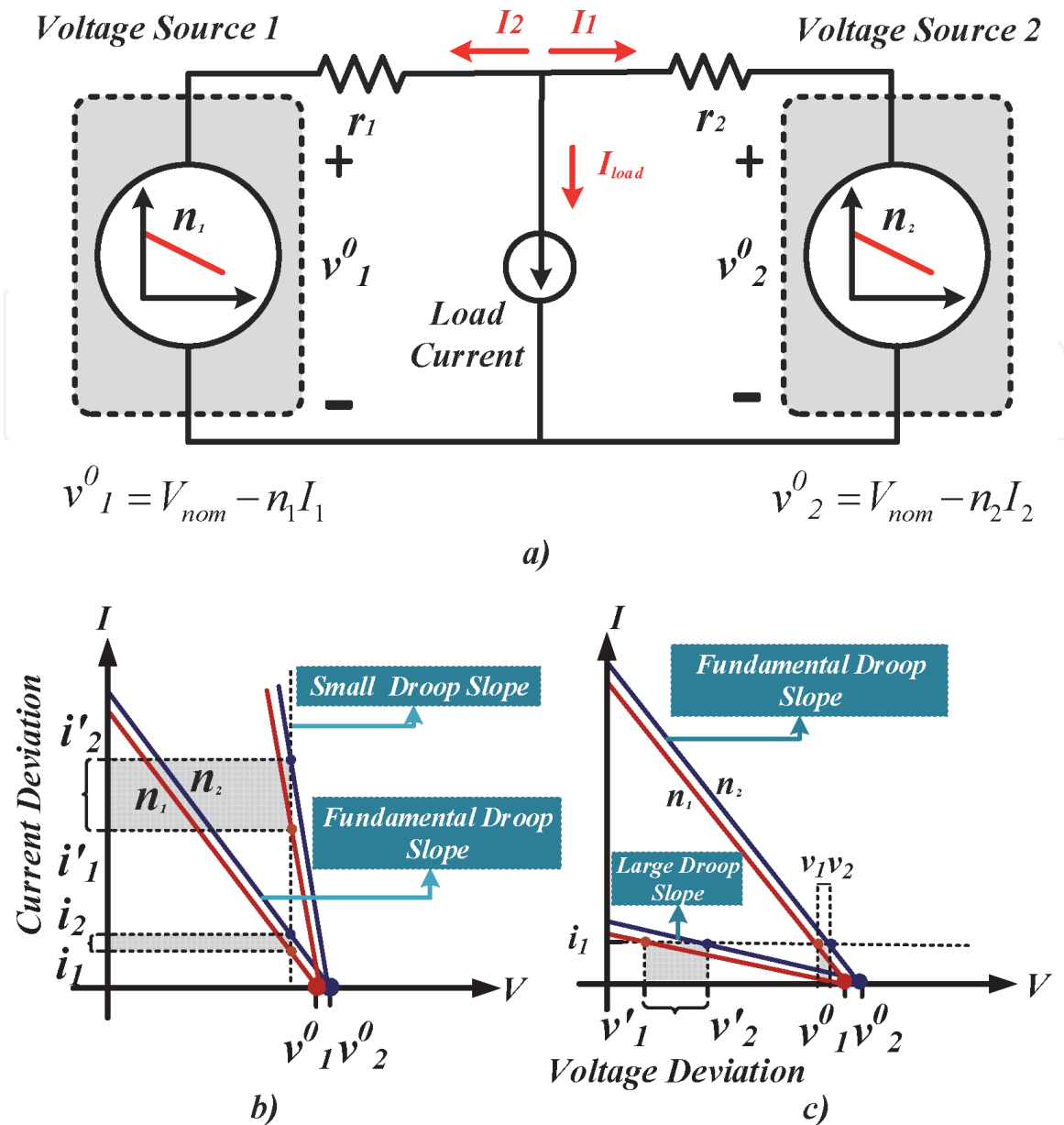
inevitably increase in the future, the need for a DC MGs will also increase. The reason is that the need for PV cells and ESSs is increasing. The advantages of the DC MGs over the AC MGs are summarized as follows [7, 8]:

1. DC MGs are more efficient and the natural fits for DC sources and loads.

2. Most of the existing challenges in AC MGs are due to reactive power flow, power quality, and frequency regulation, which do not exist in the DC MGs.

3. In terms of transmission efficiency (loss associated with the reactive current is eliminated) and power supply reliability (more reliability overall because of fewer components), DC MGs have a superior performance in comparison to AC MGs [8].

Thus, DC microgrids seem to be a natural framework for future power delivery [9].

In DC MGs, regulating the common DC-bus voltage is the main control task. To gain this goal, two different methods have been proposed in the literature [10–14], autonomous droop-based control schemes and non-autonomous centralized controllers (that are based on communication links). Droop-based methods are widely used due to their simplicity and reliability (centralized methods can not be relied upon due to their dependency on the communication links) [15–31]. However, the existing and conventional droop-based methods cannot propose an optimal performance in terms of reliability and efficiency exclusively in the islanded mode of operation. In addition, existing droop controllers usually result in large voltage variations at the DC bus during transients in the islanded mode. Large voltage fluctuations may jeopardize the system reliability and damage power electronic converters in MGs [3, 4]. However, the proper performance of linear or conventional droop controllers with a constant droop gain is reduced in light and full load conditions. This is due to a trade-off between voltage deviation and current sharing. In terms of current sharing accuracy and stabilization of Constant Power Loads (CPLs), high droop gains are preferable [11]. In term of voltage regulation low droop gains are desirable. Due to this trade-off between current sharing and voltage deviation, constant droop gains can not guarantee high performance, and it would be a big challenge. **Figure 1** shows this trade-off in the conventional droop control in a simplified DC MG's with two DC sources. It shows that constant droop gain can not be a precise and comprehensive method in both light and full load conditions [11].

To address this issue, different methods have been proposed in the literature to maintain a high level of reliability [5, 6]. A fuzzy logic strategy for energy balancing is proposed in [12]. This method is based on utilizing the virtual resistances which are calculated based on the *SoC* of each energy storage unit using fuzzy logic algorithms in the droop profile to address the reliability and energy management issues. The prominent disadvantage of this method is the high amount of voltage deviations and circulating currents. Another energy management method that is recently presented in [13] is the mode-adaptive droop controller. Although this method can alleviate the energy management issue, it is not very sensitive to the small values of voltage differences in the voltage sensors. An adaptive droop control strategy is presented in [14], which provides load sharing and circulating current minimization. This method is based on the interface resistance between the converter terminal and the DC bus. Thus, the resistance values should be known in advance or calculated, which is a relatively complex process. A distributed adaptive-droop control with battery management capability is presented in [15].

Voltage Source 1 $\qquad$ I_2 $\quad$ I_1 $\qquad$ **Voltage Source 2**

r_1 $\qquad\qquad$ r_2

n_1 $\qquad\qquad\qquad$ I_{load} $\qquad\qquad$ n_2

v^0_1 $\qquad\qquad$ v^0_2

Load Current

$$v^0_1 = V_{nom} - n_1 I_1 \qquad\qquad v^0_2 = V_{nom} - n_2 I_2$$

a)

Current Deviation

i'_2

n_1 $\quad$ n_2

Small Droop Slope

i'_1

i_2

i_1

Fundamental Droop Slope

$v^0_1 v^0_2$

b)

I

Fundamental Droop Slope

n_1 $\quad$ n_2

Large Droop Slope

i_1

$v_1 v_2$

v'_1 $\quad$ v'_2 $\quad$ $v^0_1 v^0_2$

Voltage Deviation

c)

Figure 1.
(a) A simple DC MG with two DGs, (b) the effect of small drop causes voltage deviation with current splitting error at full load, and (c) the effect of the large droop gains in voltage deviation with current sharing error under light load conditions, respectively.

In this paper investigate a new double-layer hierarchical control strategy in MG system. The primary control layer is based on an adaptive voltage-droop profile that balances the common bus voltage while maintaining the *SOCs* of batteries close to each other [15]. The second layer uses a low bandwidth communication link to perform supervisory control tasks. The communication link is used to collect the required data to calculate the adaptive virtual resistances (VRs) along with the transit criteria for changing unit-level operating modes. In comparison to the decentralized controller methods, communication-based controllers need an infrastructure along with an increase in cost and unreliability.

Three nonlinear droop control methods are proposed in [17–19]. In [17], it is claimed that the effect of sensor calibration errors and cable resistances is minimized, while it improves voltage regulation and load sharing compared to linear droop control techniques. This method adaptively adjusts the droop gains based on three novel high-order polynomial droop equations. The three methods are proposed in this research are High-Droop Gain (HDG), Polynomial Droop Curve (PDC), and Polynomial Droop Curve With Voltage Compensation (PDCVC),

which are shown in **Figure 2**. However, the chosen droop gain value in the HDG method exhibits poor current sharing near the operating point. On the other hand, the PDC method could improve load sharing near the operating point, but shows an unexpected performance in voltage regulation under heavy-loading condition. In the PDCVC method, both current sharing and voltage regulation are improved except near no-load conditions. Two important factors were not considered in this paper, the impact of output impedance on the stability of the whole DC MG and the impact of droop control on the efficiency of system. Later in [18], a split droop controller is investigated, which droop gain can be calculated based on voltage error measurement. This strategy calculates several different slopes for each load conditions to reduce the current sharing and voltage deviation errors, which shows this task well implemented. However, differences between droop slopes create switching modes, which will be abrupt. The sudden changes in output resistance of the power converters may lead to undesired transients and oscillations. In [19], the performance of the different second order droop expressions namely parabola and ellipse droop as nonlinear droop control methods are evaluated and compared with the linear droop. The parabola and ellipse droop equations showed a good performance in both load sharing and voltage regulation but a weak performance with negative current [16]. A nonlinear programmable droop method for a low-voltage DC MG is proposed in [20] considering the effects of line resistances and the state of charge of the batteries in the power- sharing process. This method has been able to reduce the impacts of sensor and cable errors at heavy load. It also reduces the voltage variation while load sharing is still guaranteed. However this method does not have a good performance, when the converter output current is negative. Moreover, under light-loading conditions, the values of droop gain lead to creating poor load sharing [20].

In this paper a novel control system has been proposed to improve the reliability and efficiency of DC micro-grids operating in the islanded mode. **Figure 3** shows the block diagram of the DC MG considered in this paper. Two energy storage systems along with two solar energy harvesting systems are connected to the DC bus to feed 4 kW DC loads. The focus of this paper is on small scale DC micro-grids for residential applications, which means the line impedance can be negligible [14, 19]. The main contribution to this article is that the proposed control system allows RESs to operate at their maximum power point whenever it's possible. The main advantage of the proposed control system is that the MG can optimally utilize energy storage system in conjunction with renewable energy systems. Additionally, the proposed control system can maintain tight regulation of the DC bus voltage within a predefined range. Unlike the aforementioned nonlinear methods, the presented method has a precise performance in negative current (when the output
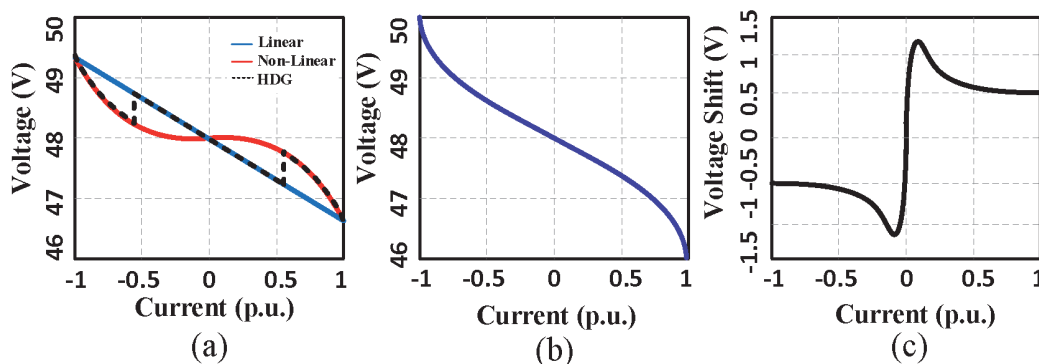
Figure 2.
(a) Droop characteristics for HDG method, (b) droop characteristics for PDC method, and (c) Δv curve for PDCVC method.
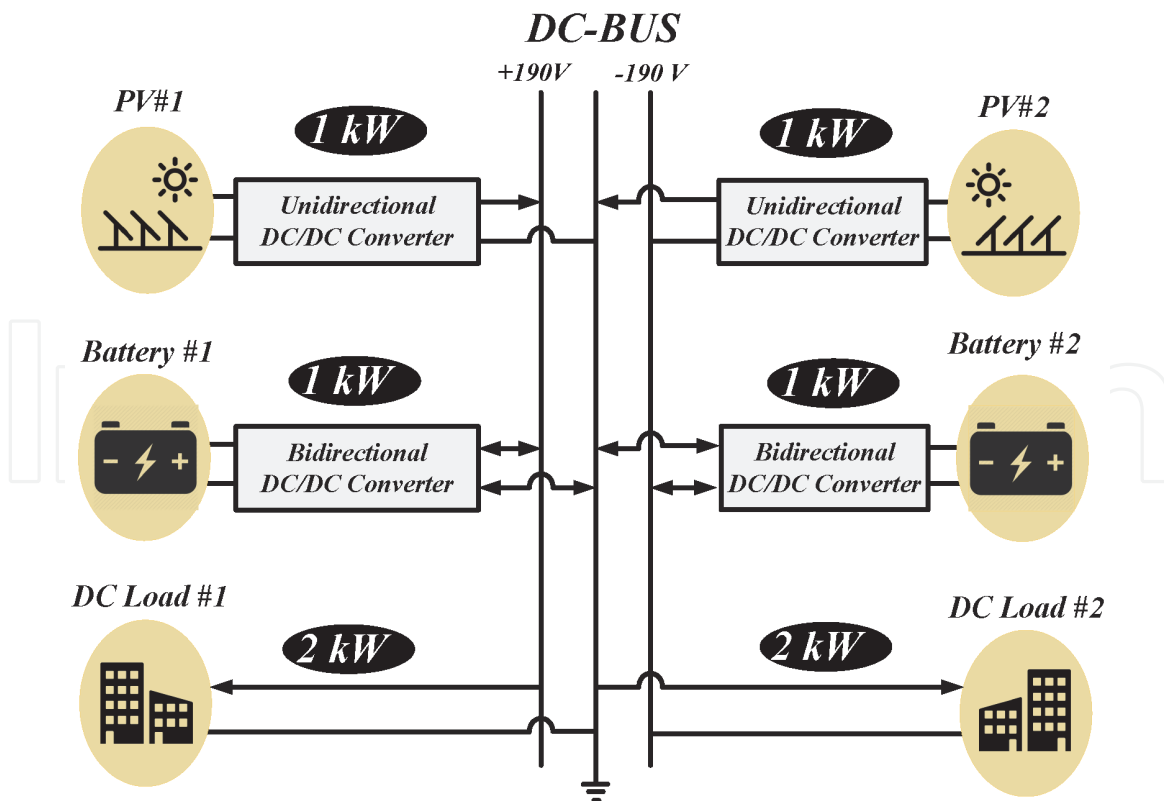
Figure 3.
DC microgrid configuration (implemented system).

power is absorbed by the battery) which is similar to the positive current (when the battery converter injects power to the MG). The calculations of the droop gain in the proposed method are independent of the measured output current. Therefore, this method immunizes the proposed control system from current ripples and sensor errors in comparison to the methods with high order polynomial droop methods. This method has an ability to change the droop gain smoothly from light load to full load conditions, without switching modes resulting in no abrupt in the control system. Voltage deviation and current sharing improved in this method in comparison to other nonlinear and conventional droop control, and it will be shown and explain in the following section. This method has been implemented and analyzed in the Micro-Grid systems due to this fact, the most difficult tasks and challenges have occurred in the MG system, not in the grid- connected system. In the grid-connected system the bus voltage is constant with less complexity and less non-ideal elements or parameters. Various power flow scenarios have been analyzed to verify the performance of the MG.

This paper is organized as follows. The proposed control system and various operating scenarios are described in Section 2, respectively. Moreover, two sub-sections called the definition and ranges of the adaptive parameter are added in Section 2. In Section 3, the optimal selection of the the adaptive parameters is presented. The stability analysis performed in Section 4. Finally the simulation and experimental results are presented in Section 5.
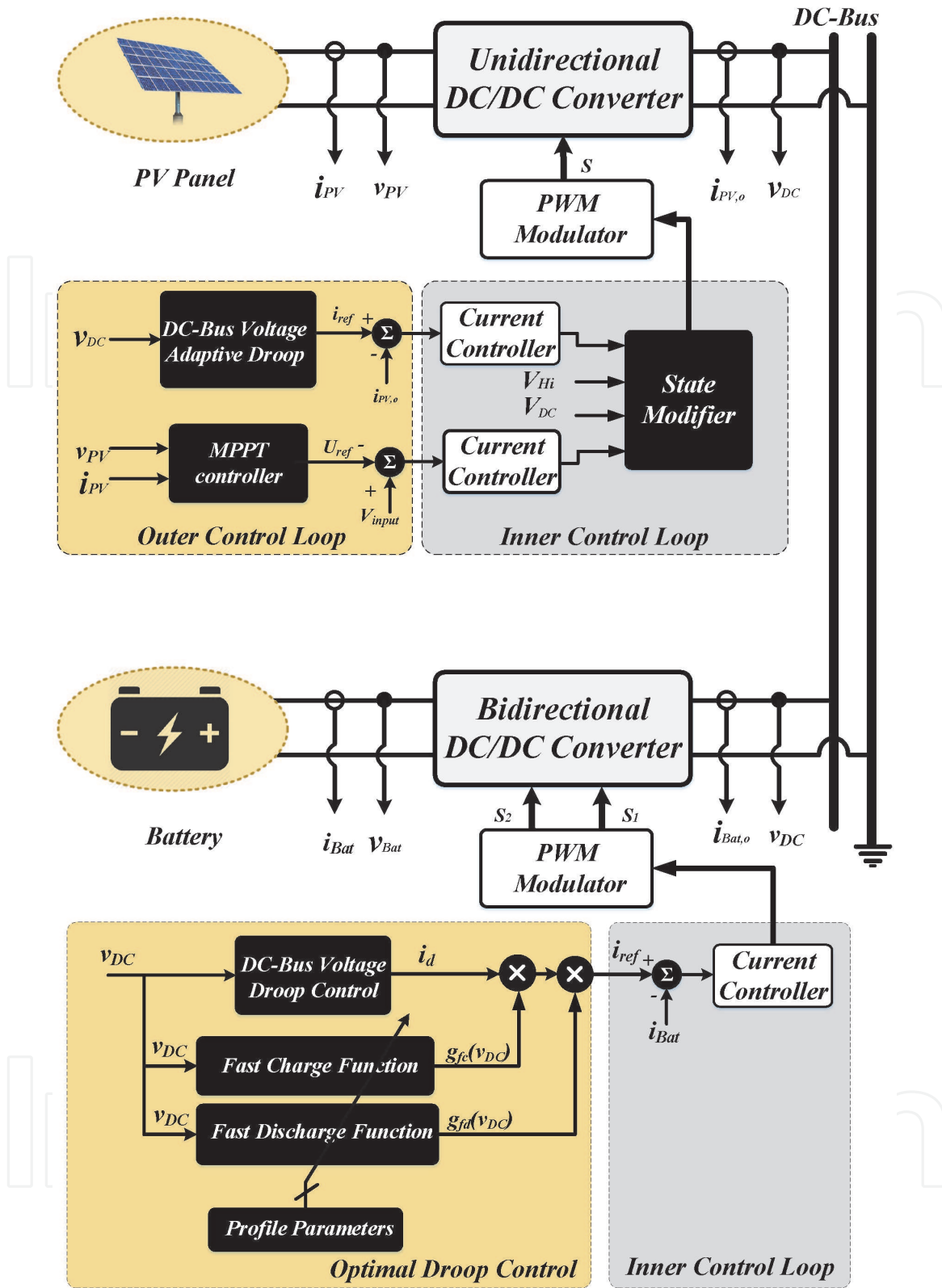
2. Proposed Control System

In order to describe the performance of the proposed control system in all operation modes, a scenario will be discussed. Energy devices and systems in which the solar system and battery are connected to the grid/load through power converters have four operating modes which are listed as follows:

1. Grid-connected mode: When the system is connected to the grid, in order to transmit the maximum power, the power converter connected to the solar cells performs maximum power point tracking (MPPT). During this mode, the battery's state of charge should be controlled so that when the system is disconnected from the grid and turns into an island system, the battery has enough energy to supply the island system. Therefore, in accordance with the battery's state of charge, the battery is charged or discharged, which are two modes of operation.

2. Island mode: In this mode, the power converter connected to the solar cells still performs MPPT. During this mode of operation, the DC-bus voltage should be kept constant (within the range of 10%) by the power converter; whereas, in grid-connected mode, the voltage of DC-bus is relatively constant for various conditions. Therefore, to achieve power-sharing and load voltage regulation, the battery connected power converter is controlled with the droop control method. For instance, if the load voltage decreases, battery is discharged to transmit more power; and when the load voltage increases, power is transmitted back to the battery and charges it.

3. Special case of island mode: If the battery is fully charged/discharged during the island mode, the power-sharing and output voltage regulation are achieved by the solar connected power system. Hence the power system evades MPPT and is controlled with the droop control method.

In the islanded mode of operation, one of the main problems with the existing droop-based controller is that the MG components are not utilized in an efficient manner [30, 31]. For example, in several scenarios, to keep the stability of the system, renewable energy sources must deviate from their maximum PowerPoint [30, 31]. The main contribution of this method shows the presented control system allows RESs to operate at their maximum power point whenever it can be possible. **Figure 4** shows the general block diagram of the proposed control systems for the solar energy harvesting system and the energy storage system (ESS) in the DC MG. The solar control system consists of one MPPT control and one adaptive droop control, which are separated from each other by a state modifier. The structure of the solar control system will be discussed in the next paragraph. After that, the battery control system will be discussed in details as the main proposed control method. The battery control system consists of a supervisory adaptive droop control to manage energy through the DC MG system. The optimal utilization is performed through incorporating the adaptive charge/discharge terms to the control system of the ESS. These terms implement a nonlinear adaptive droop profile for the ESS in order to perform a tighter voltage regulation. Moreover, due to working in a high level of power (More than 100 W), all the analysis are preferred in continues conduction modes, because working in discontinuous conduction mode in high-level power comes with high peak current and power loss, which it is not desired.

According to **Figure 5**, the schematic of the solar controller along with its boost converter is illustrated. The outer control loop of the solar energy harvesting system consists of two blocks: the MPPT controller that ensures maximum power is extracted from the solar module, and the adaptive DC-bus voltage controller. The switching between these two control algorithms is preformed by the state modifier block as follows:

$$\begin{cases} if \ \ V_L \leq \ v_{DC} \leq \ V_H \Rightarrow State \coloneqq MPPT \ Mode \\ Otherwise \Rightarrow State \coloneqq Droop \ Mode \end{cases} \tag{1}$$
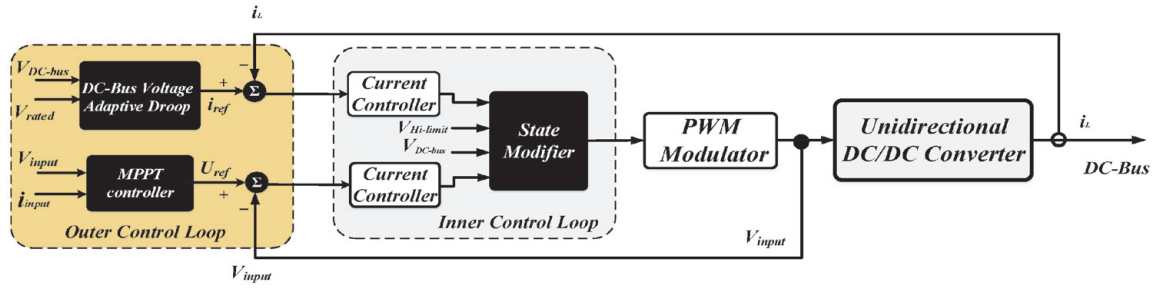
Figure 4.
Block diagram of the proposed control scheme for PV units and energy storage systems in DC MG.

where V_L and V_H are defined based on the MG requirements and safety standards [29]. This structure provides flexibility to operate at the MPPT as much as possible.

The block diagram of the ESS is discussed according to the **Figure 4**. In this figure, the presented control method offers four modes of operations: charging mode, discharging mode, fast charging mode, and fast discharging mode while the conventional droop control method offers only, charging mode and discharging

Figure 5.
The block diagram of control system in solar converter.

mode. Using the two extra modes, the control system is able to offer voltage regulation, while improving the reliability of the system. The outer loop produces a reference value for the inner current control loop. The outer loop is optimized droop controller that incorporates two extra modes (i.e., fast charge, and fast discharge) into the control system. These modes are incorporated through two nonlinear functions, $g_{f_c}(v), g_{fd}(v)$ (*fc*) stands for fast charge and (*fd*) is short for "fast discharge"). These functions effectively determine the speed of charge and discharge of the battery based on the DC-bus voltage.

Control systems based on optimization methods can be the proper solutions in determining the critical and unknown parameters of the MG systems [28, 29]. According to **Figure 3**, the optimal droop controller produces the reference value for the output current of the ESS. This current is given by:

$$i_{ref} = i_d(v_{DC})g_{f_c}(v_{DC})g_{fd}(v_{DC}) \qquad (2)$$

The reference current includes three terms. The first term is produced by the DC-bus voltage droop controller given by:

$$i_d = -k_D \times (V_{nom} - v_{DC}) \qquad (3)$$

where k_D, V_{nom}, v_{DC}, and i_{ref} are the droop coefficient, the nominal voltage value, the DC-bus voltage, and the reference current respectively.

2.1 Adaptive parameters definition

The other two terms, $g_{f_c}(v), g_{fd}(v)$, represented in Eq. (2) are the adaptive functions for the fast charging and fast discharging modes, given by (when $V_{min} \leq v_{DC} \leq V_{max}$):

$$g_{f_c}(v_{DC}) = \exp\left(\frac{(v_{DC} - V_{fc})}{\alpha_{fc}} u(v_{DC} - V_{fc})\right) \qquad (4)$$

$$g_{fd}(v_{DC}) = \exp\left(\frac{(V_{fd} - v_{DC})}{\alpha_{fd}} u(V_{fd} - v_{DC})\right) \qquad (5)$$

where $\exp(.)$ is the exponential function, $u(.)$ is the unit step function, V_{fd} and V_{fc} both determine the start points of fast charging and fast discharging modes respectively, and α_{fc} and α_{fd} are the exponential coefficients to create fast charging and fast discharging respectively.

Figure 6 shows the way to calculate the current reference based on the DC-bus voltage for the Battery or ESS. This figure shows, the proposed controller provides two extra modes (i.e., fast charge and fast discharge), when the DC-bus voltage is lower than V_{fd} or higher than V_{fc}. When the DC-bus voltage is lower than V_{fd}, it means that the load is too heavy and the ESS needs to inject much more power to sustain the DC-bus voltage. When the DC-bus voltage is higher than V_{fc}, it means that the generation is higher than the load. Thus, the extra power is used to fast charge the battery. The adaptive droop profiles go through the fast charge/ discharge modes when the step functions are equal to one. This function allows the control system to absorb and inject more power than the conventional system automatically to prevent the voltage deviation. **Figure 7** shows the performance of the proposed droop profile in current sharing and voltage deviation in a DC MG with two DC sources. Even in the worst case (when the droop gain in the two DC sources is considered equal and constant) the current sharing and voltage deviations are improved reasonably in comparison to the conventional ones in **Figure 1**.

2.2 Adaptive parameters range

In order to achieve a stable and reliable system, the limitation on the numerical domain of Eq. (2) should be considered. The aforementioned limitation is set to meet the requirements of the implemented control system. The considered limitation, which is defined according to voltage regulation range, resources power rating, and load demanded power, will be discussed in detail as follows. In the **Table 1** all the implemented components and variables are listed. The natural Logarithm domain and charge/discharge rate limitations of the implemented batteries, specified the values of α_{fd}, α_{fc}, V_{fc}, and V_{fd}. According to the simulation of the proposed control system in PSIM software and charge/discharge rate limitations of the
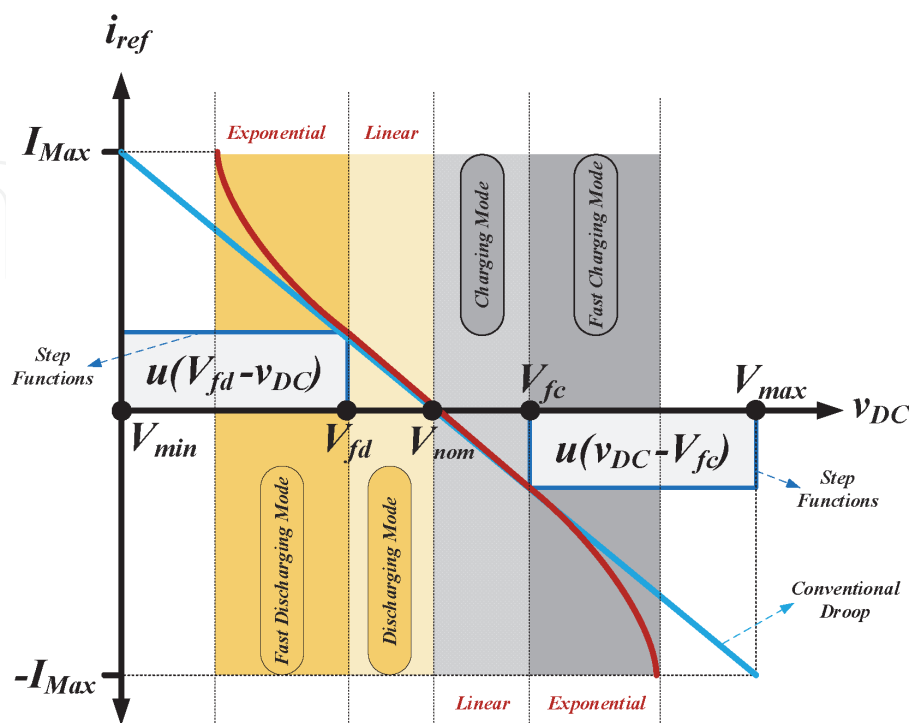
Figure 6.
The performance of the step and exponential functions in the proposed controller.
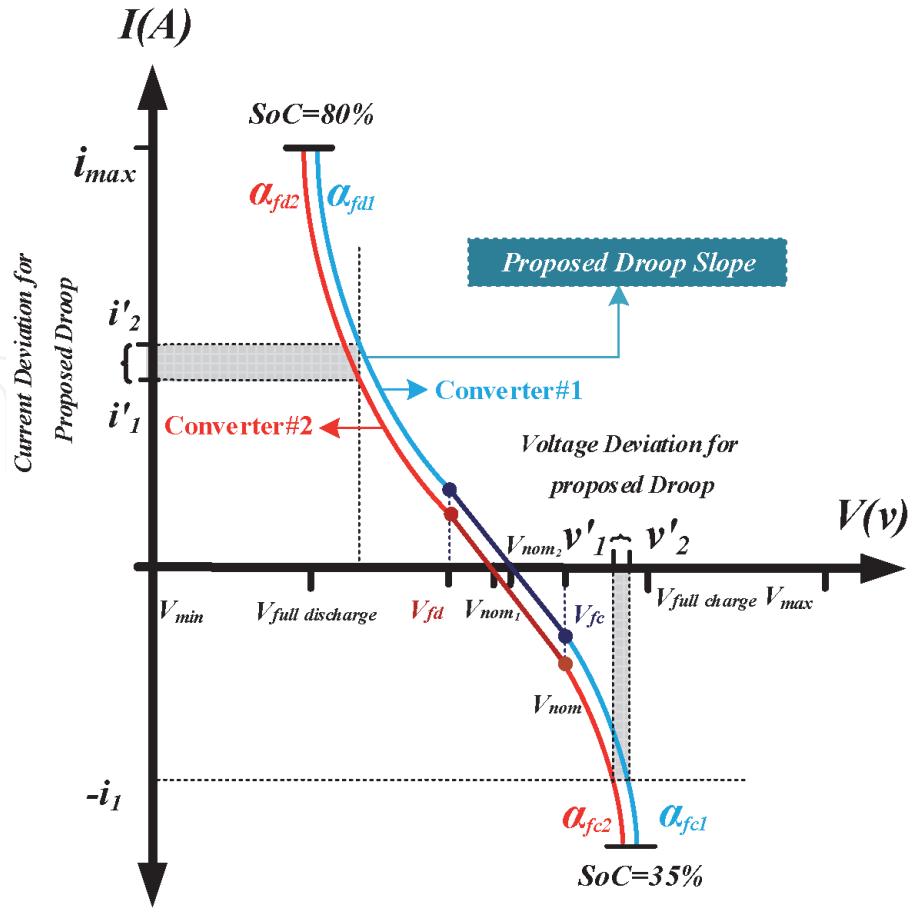
Figure 7.
The current sharing and voltage deviations in the proposed system in comparison to the conventional one in
Figure 2.

Symbols	Parameters	Values
P_o	Nominal Output Power for Battery#1 converter	1 kW
P_o	Nominal Output Power for Battery#2 converter	1 kW
P_o	Nominal Output Power for PV#1 converter	1 kW
P_o	Nominal Output Power for PV#2 converter	1 kW
f_{sw}	Switching Frequency	100 kHz
V_{nom}	Nominal DC MG Voltage	190 V DC
$V_{in_{Bat}}$	Battery Bank Voltage	80 V DC
$V_{in_{PV}}$	PV Bank Voltage	80 V DC
L_1	Battery input Inductor	$150\mu H$
L_2	PV input Inductor	$330\mu H$
C_o	Output Capacitor	$200\mu F$

Table 1.
DC/DC converter specifications in simulation.

batteries, lower range of α_{fd} and α_{fc} have to be specified to ensure the reliable operation of the system in all operating conditions as follow:

$$\alpha_{fc} \geq 2.9, \tag{6}$$

$$\alpha_{fd} \geq 2.9, \tag{7}$$

The upper range of α_{fd} and α_{fc} are specified based on the voltage regulation range and minimum fluctuations around the rated voltage (to achieve this goal, the $V_{fc_{Min}}$ and $V_{fd_{Max}}$ must be specified to keep the minimum distance from the rated voltage). The aforementioned upper ranges are given as:

$$i_{d_{Max}} = -k_D \times (V_{nom} - v_{DC_{Max}}) \times g_{fc}(v_{DC_{Max}})\Big|_{V_{fc_{Min}}} \tag{8}$$

$$i_{d_{Max}} = -k_D \times (V_{nom} - v_{DC_{Min}}) \times g_{fd}(v_{DC_{Min}})\Big|_{V_{fd_{Max}}} \tag{9}$$

Finally the upper and lower range of α_{fd} and α_{fc} are:

$$2.9 \le \alpha_{fc} \le 12.8, \tag{10}$$

$$2.9 \le \alpha_{fd} \le 12.8, \tag{11}$$

In the implemented control system, the proposed range of the DC-bus voltage is considered to be $180 \le v_{DC-bus} \le 200$. Thus, the ranges for the fast charge/discharge voltages are given by:

$$V_{fd} \ge \alpha_{fd_{Min}} \times Min \left| \ln \frac{i_{ref} \times SoC(t)}{(-k_D \times (V_{nom} - v_{DC}))} \right| + v_{DC_{Min}} \tag{12}$$
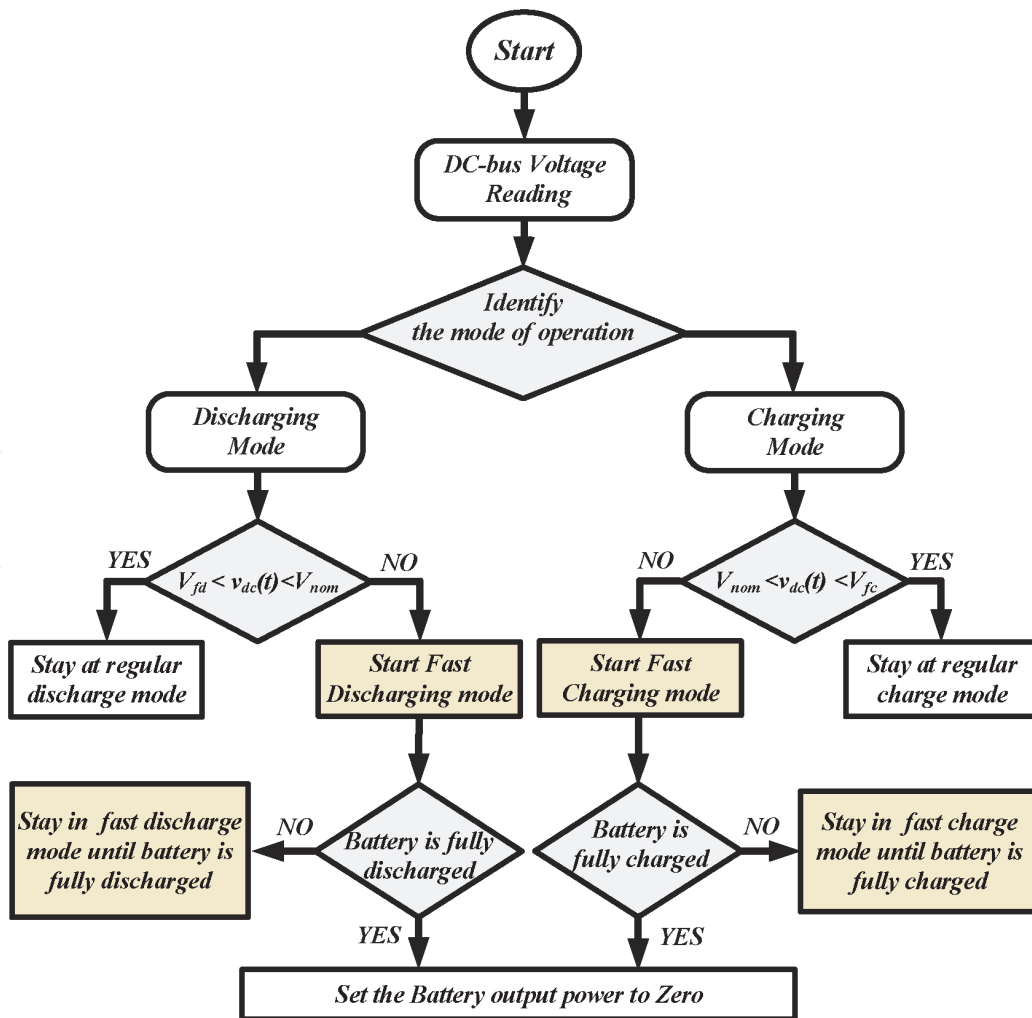
Figure 8.
The flowchart of the proposed control scheme for the ESS.
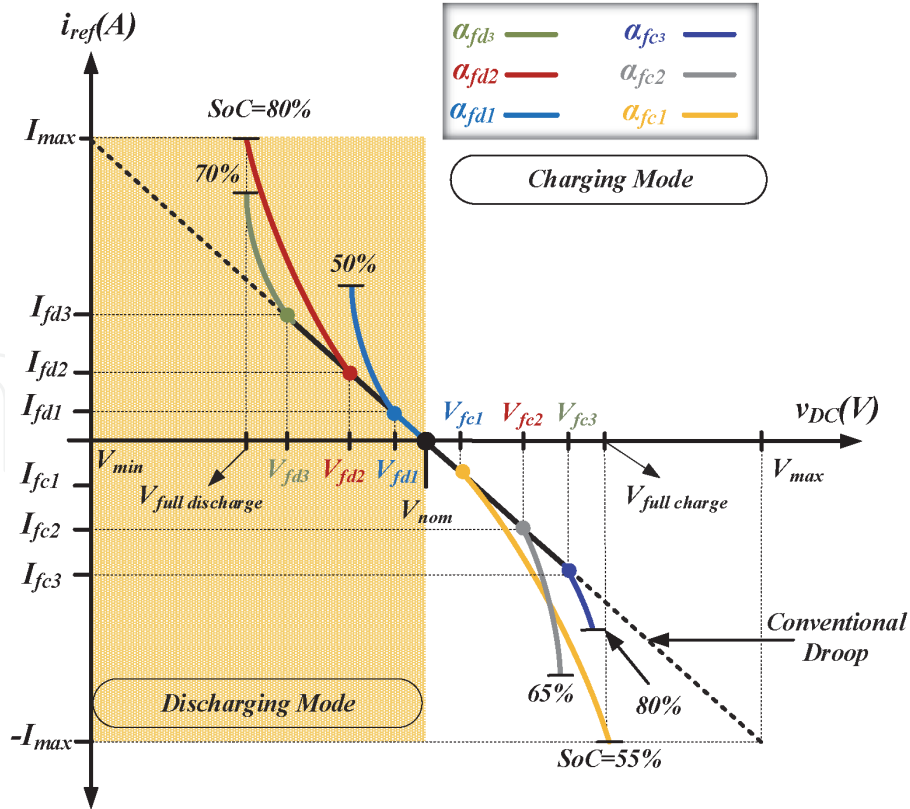
Figure 9.
Proposed adaptive droop controller with adaptive charge/discharge functions.

and

$$V_{fc} \geq v_{DC_{Max}}$$

$$-\alpha_{fc_{Min}} \times Max \left| \ln \frac{-i_{ref} \times SoC(t)}{(-k_D \times (V_{nom} - v_{DC}))} \right| \tag{13}$$

Therefor, the upper and lower range of V_{fd} and V_{fc} are:

$$191 \leq v_{fc} \leq 198, \tag{14}$$

$$182 \leq v_{fd} \leq 189, \tag{15}$$

The main advantages of the profile proposed in **Figure 5** are twofold. It provides a much better dynamical result for the ESS to utilize the available energy optimally. It also provides a small margin in the range of DC-bus voltage or its variations. Thus, it gives a chance for the converters to operates more optimally. The proper voltage deviation and desired power-sharing can be achieved by this method adaptively and autonomously, without any switching modes which lead to the harsh transients. **Figure 8** shows the flowchart of the control system for ESS. This figure shows how various modes of operation get activated by the DC-bus voltage. The (*SOC*) of the battery should be considered as a very important factor in selecting different parameters. **Figure 9** depicts different profiles in the various *SOC* values. In **Figure 9** charging and discharging is determined by the battery conditions to maintain the bus voltage.

3. Optimal droop control parameters

In this section, the procedure to determine the optimal values of the parameters for the proposed optimal droop controller is described. The objective is to find

appropriate values for four parameters: V_{fc}, V_{fd}, α_{fc}, and α_{fd}. The *SOC* of the ESS plays a very important role in the calculation of the adaptive parameters. An optimization algorithm to determine the precise values for the speed and depth of charge/discharge is the main idea of this method.

The proposed algorithm is based on sequential quadratic programming (SQP) [33], which is an iterative method for nonlinear optimizations. It can handle any degree of non-linearity, including non-linearity in the constraints [32]. **Figure 10** shows the block diagram of the energy storage system with the proposed control system with the all details. This diagram shows the nonlinear optimization block with its inputs and outputs. **Figure 11** shows that the SQP algorithm calculates the optimal values for the adaptive parameters. The proposed controller uses these values to generate the nonlinear functions $g_{fc}(v_{DC})$ and $g_{fd}(v_{DC})$. The following steps are implemented in the SQP algorithm:

1. The optimization variables are defined as:

$$X = \begin{bmatrix} x_1 \\ x_2 \\ x_3 \\ x_4 \end{bmatrix} = \begin{bmatrix} \Delta V_{fd} \\ \alpha_{fd} \\ \Delta V_{fc} \\ \alpha_{fc} \end{bmatrix} \tag{16}$$

where $\Delta V_{fd} = V_{fd} - V_{nom}$ and $\Delta V_{fc} = V_{fc} - V_{nom}$. As written in Eq. (16), the four optimization variables are ΔV_{fd}, ΔV_{fc}, α_{fd}, and α_{fc}. The reason for choosing these four optimization variables is that in each value of *SoC*, the control system will determine a new optimum point in the charge and discharge modes of operation. This task can not be possible without these main variables. For reliable
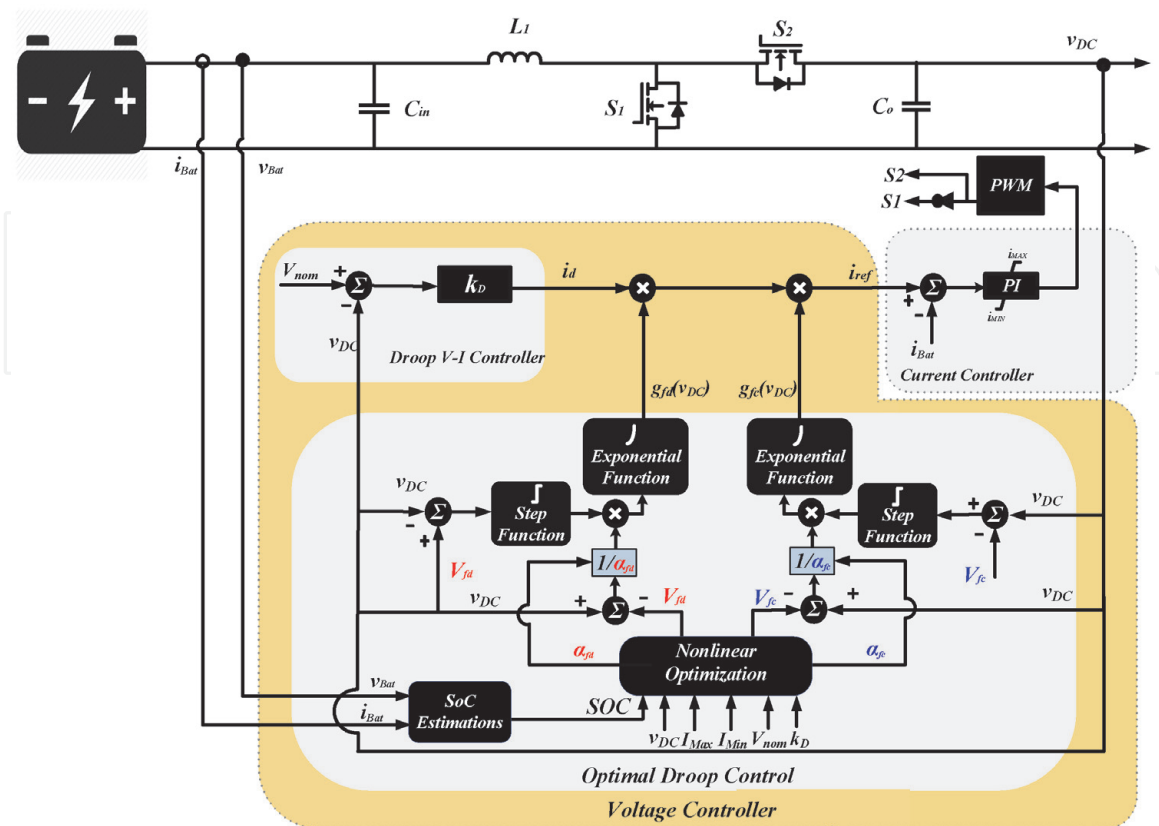
Figure 10.
The DC/DC converter for the ESS with its control system.
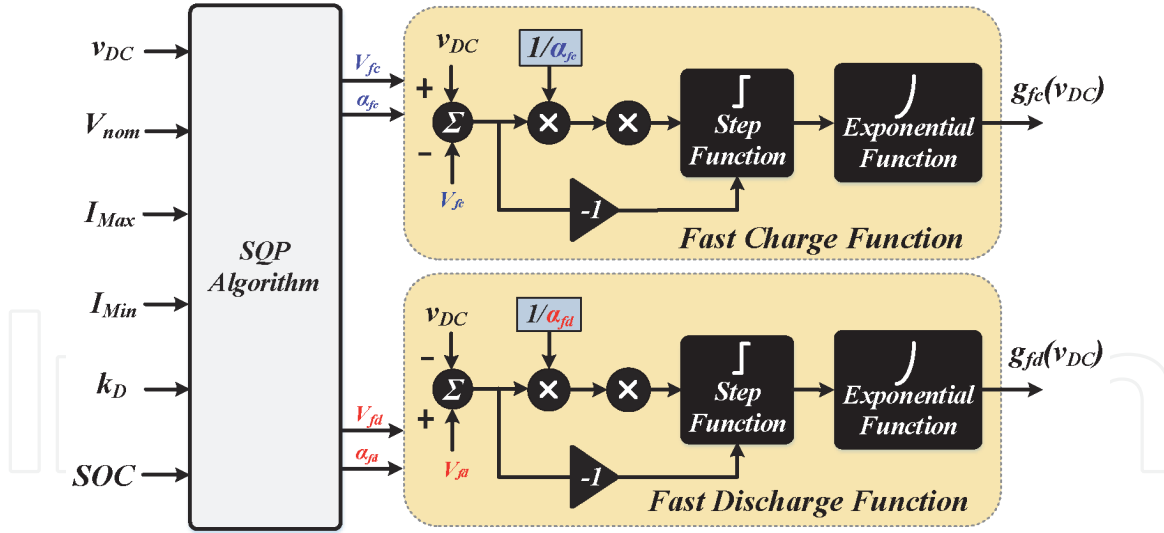
Figure 11.
Structure of charge/discharge control functions in the proposed method.

performance, three sensitive cases are proposed for system decisions in the optimization process. Two cases occur when the *SoC* value is high in discharging and charging modes, and another is when the value of *SoC* is low. For instance in discharge mode, the values of two variables (α_{fd} and ΔV_{fd}) with the highest *SoC* value will be specified by the optimization algorithm when α_{fd} has its minimum value and ΔV_{fd} has its maximum value. This decision is helpful to discharge the battery smoothly during a long time while achieving less voltage deviation.

2. The general form of the objective function is defined as:

$$SQP : \begin{cases} Minimize \ f(X) \\ \\ Subject \ to : \begin{cases} H_{eq}(X) = 0 \\ \\ H_{ineq}(X) \leq 0 \end{cases} \end{cases} \tag{17}$$

where $H_{ineq}(X)$ and $H_{eq}(X)$ are the inequality and equality constraints. In the proposed adaptive droop control, only two inequality constraints H_{fd}, and H_{fc} are defined as shown in Eqs. (18) and (19). This optimization program lacks the equality constraints, due to current or power changes in droop profile. In this particular optimization problems, the following constraints are considered:

$$H_{fd}\left(\Delta V_{fd}, \alpha_{fd}\right) = k_D \times (V_{nom} - v_{DC}(t))$$

$$\times e^{u\left(-v_{DC}(t) - \Delta V_{fd} + V_{nom}\right) \times \frac{\left(-v_{DC}(t) - \Delta V_{fd} + V_{nom}\right)}{\alpha_{fd}}} - I_{max} \leq 0 \tag{18}$$

$$H_{fc}\left(\Delta V_{fc}, \alpha_{fc}\right) = I_{min} - k_D \times (V_{nom} - v_{DC}(t))$$

$$\times e^{u\left(-v_{DC}(t) + \Delta V_{fc} - V_{nom}\right) \times \frac{\left(-v_{DC}(t) + \Delta V_{fc} - V_{nom}\right)}{\alpha_{fc}}} \leq 0 \tag{19}$$

Having two modes of operation (charge and discharge modes) and more than one optimization variable, the need for the cost function to optimize more than one variable simultaneously, will be increased. The cost functions for this optimization problem are defined as:

1. Discharging mode:

$$f_1(x) = \Delta V_{fd} = V_{fd} - V_{nom} \tag{20}$$

$$f_2(x) = \alpha_{fd} \tag{21}$$

2. Charging mode:

$$f_1(x) = \Delta V_{fc} = V_{fc} - V_{nom} \tag{22}$$

$$f_2(x) = \alpha_{fc} \tag{23}$$

The total cost function is defined as the weighted sum of the aforementioned functions given by:

$$f(x) = \sum_{m=1}^{2} w_m f_m(x) = w_1 f_1(x) + w_2 f_2(x) \tag{24}$$

where w_1 and w_2 are the coefficients utilized to determine the role of each function in the nonlinear optimization algorithm.

The *SOC* of the battery is also incorporated into the optimization algorithm. The multi-objective optimization function is modified to incorporate the *SOC*:

1. Case 1:

$$(Discharge\ mode)$$

$$if\ SOC \leq 40\% \tag{25}$$

$$Maximize\ f(x) = w_1 \Delta V_{fd} + w_2 \alpha_{fd}$$

2. Case 2:

$$(Discharge\ mode)$$

$$if\ SOC \geq 40\% \tag{26}$$

$$Minimize\ f(x) = w_1 \Delta V_{fd} - w_2 \alpha_{fd}$$

3. Case 3:

$$(Charge\ mode)$$

$$for\ all\ SOC\ values \tag{27}$$

$$Minimize\ f(x) = w_1 \Delta V_{fc} - w_2 \alpha_{fc}$$

According to (25) and (26), two operating cases have been considered for the discharge mode based on *SOC* values. In case one, the storage system needs to be discharged as slow as possible to prevent storage capacity depletion. This can be done by maximizing $f_1(x)$, and $f_2(x)$. In Case two, simulates the discharging mode when the *SOC* is more than 40%. In this case, the optimization algorithm tries to maximize $f_2(x)$ while minimizing $f_1(x)$. Also, the Eq. (27) is defined for the cases with all *SOC* values in charge mode, which means the controller system always tends to charge the ESS as fast as possible. **Figure 12** shows an exemplary optimization in case one with $SOC = 20\%$. In this figure, the total function evaluations are
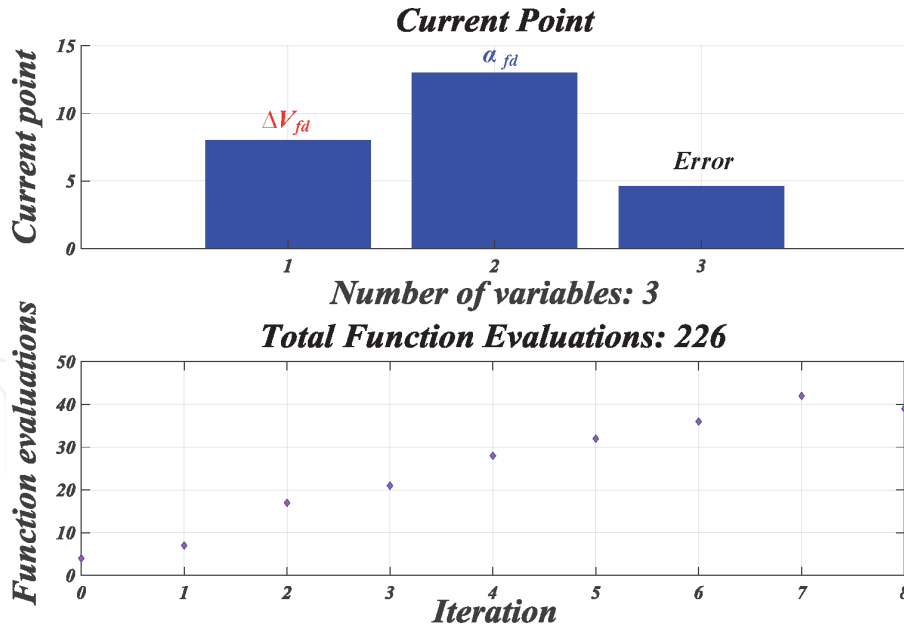
Figure 12.
*An example of SQP algorithm performance in the situation of SOC = 20%.*

226 which means around 226 intermediate calculations take place to reach to the next optimum solution during 8 times iterations. After 8 iterations the optimization process stops. There is an initial error-check that evaluates the objective function before any iterations take place. Three variables are defined in this figure, which are ΔV_{fc}, α_{fc}, and Error. In the case of $SOC = 20\%$ the optimum solutions are calculated for these three variables 8, 13, 5 respectively. The optimum solutions show that for this SoC the control system performs like the conventional droop in order to not missing the remaining power in the battery so fast.

4. Stability analysis

In this section, the stability analysis of the proposed control method is performed. The proposed optimal droop control system utilizes profiles with linear and nonlinear parts. When the system operates in the linear part (i.e., conventional droop profile), the stability analysis is straight forward. However, nonlinear methods (e.g. the Lyapunov stability theory) must be used to analyze the stability of the nonlinear part (the stability analysis has been carried out only for the islanded mode of operation) [34, 35].

Figure 13 shows the block diagram of the closed-loop control systems and the schematic diagram of the converter. According to **Figure 13**, the dynamical model of the battery is also considered in the schematic block diagram. According to **Figure 13**, the state-space model of the ESS is given by [29]:

$$
\begin{cases}
\dfrac{di_L}{dt} = \dfrac{1}{L} v_{C_{in}} - \dfrac{1}{L} v_{DC}.d' \\[2mm]
\dfrac{dv_{DC}}{dt} = \dfrac{1}{C_o}.d'.i_L - \dfrac{1}{C_o.R_{eq}} v_{DC} \\[2mm]
\dfrac{dv_{C_b}}{dt} = \dfrac{V_{oc} - v_{Cb} - v_{C_{in}}}{C_b.R_{sb}} - \dfrac{v_{C_b}}{C_b.R_b} \\[2mm]
\dfrac{dv_{C_{in}}}{dt} = \dfrac{V_{oc} - v_{Cb} - v_{C_{in}}}{C_{in}.R_{sb}} - \dfrac{i_L}{C_{in}}
\end{cases}
\tag{28}
$$
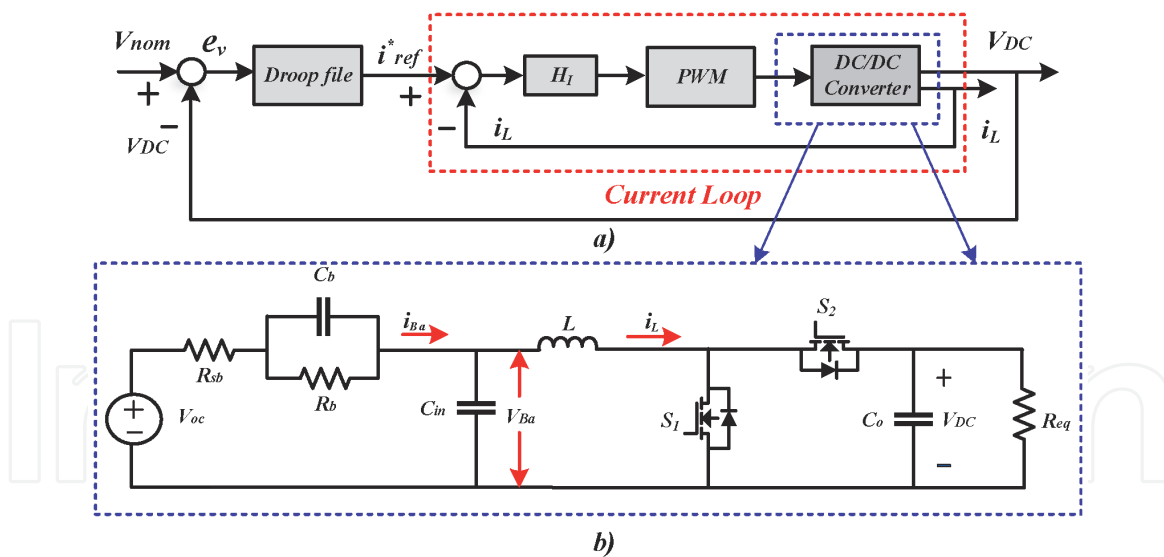
Figure 13.
(a) Closed-Loop block diagram of the battery controller. (b) DC-DC converter schematic.

where, C_{in}, C_b, C_o, R_{eq}, R_{sb}, and L are the input capacitor of the DC/DC converter, the equivalent series capacitor in the battery model, the DC/DC converter output capacitor of battery, the MG side equivalent load, and the DC/DC converter input inductor. v_{DC}, $v_{C_{in}}$, v_{C_b}, i_L, and i_{Ba} are the DC bus voltage, the input voltage of the DC/DC converter, the voltage across C_b, the inductor current and the input current of the battery respectively. Also, $d' = 1 - d$, where d is duty cycle.

According to (28), the system dynamics include fast changing current, i_L, and slow changing voltages, v_{DC}, $v_{C_{in}}$, v_{C_b}. Due to different rates of changes, the cascade control system shown in **Figure 13** includes the fast inner current loop and the slow outer voltage loop. The two loops can be divided into two parts with different rates of change, as the current control loop has much faster dynamics than the comparatively slow voltage control loop. The current control loop has is called the fast boundary layer and the voltage loop is named the slow quasi-steady state. In order to analyze the stability of this cascade control loop, the dynamics of the system are separated into the slow dynamics and the fast dynamics.

According to (28) and **Figure 13**, the dynamics of the DC/DC converter for the current loop is given by:

$$\frac{di_L}{dt} = \frac{1}{L}v_{C_{in}} - \frac{1}{L}v_{DC}.d' \tag{29}$$

In (29), v_{DC}, $v_{C_{in}}$ are slow varying relative to the current and considered constants in this equation. In order to design the controller the following Lyapunov function is defined:

$$V_i = \frac{1}{2}e_i^2 \tag{30}$$

where $e_i = i_{ref} - i_L$. By considering (29) and (30), the following controller renders the derivative of the Lyapunov function negative definite:

$$d' = \frac{V_{Cin}}{V_{DC}} - k_p e_i - k_i \int e_i \tag{31}$$

According to **Figure 13**, the voltage loop includes the nonlinear droop block and the closed loop block of the inner current control loop. It is worthwhile to mention

that the voltage loop does not try to render the voltage error zero. Thus, the asymptotic stability is not required and the boundedness of the voltage variables is the only requirement. In order to investigate the boundedness, the energy function for the voltage error signal is defined as:

$$V_v = \frac{1}{2} \times e_v^2 \tag{32}$$

where $e_v = V_{nom} - v_{DC}$.

According to (28) the dynamics of the voltage error is given by (due to the fast varying current loop, it is assumed that the inductor current and duty cycle have already reached their final values):

$$\frac{de_v}{dt} = \frac{1}{C_o . R_{eq}}(V_{nom} - e_v) - \frac{1}{C_o}.D'.I_L \tag{33}$$

The derivative of the energy function (32) is given by:

$$\dot{V}_v = \dot{e}_v \times e_v = \frac{1}{C_o . R_{eq}} \left[(V_{nom} - D'.I_L.R_{eq})e_v - e_v^2 \right] \tag{34}$$

due to the fact that $\left(V_{nom} - D'.I_L.R_{eq} \right)$ is close to zero the derivative of the energy function is negative. Thus the voltage error is bounded.

5. Simulation and experimental results

Simulation and experimental results are presented in this section. In **Tables 1** and **2** the specifications of the DC/DC converter used in the experimental prototype and simulations software are given in.

The DC MG configuration is shown in **Figure 3** which implemented to obtain the simulation results. The concept of dropbased control is based on reducing the voltage deviation caused by the change in MG load. Therefore, to simulate voltage deviation, two types of step change are applied in MG Load. The performance of the proposed control system is compared with the conventional drop-down method in reducing the MG voltage deviation. All the simulation results are implemented with $SoC = 80\%$. **Figure 14** shows the first type of step changes in DC MG loads in both charge/discharge modes. To illustrate and compare the performance of the proposed method with the conventional in term of power absorption and injection. As can be seen, the power absorption and induction of the proposed method is very significant in regulating the voltage which is presented in **Figure 15**. **Figure 16** shows a superior performance of the proposed method in voltage deviation by changing the DC MG load in both charge and discharge modes. **Figure 17** shows the second type of variations of the DC load inside MG for both charge/discharge modes. **Figures 18** and **19** shows the SOC value changes based on the type 2 load changes over the simulation time for the conventional and the proposed method, respectively. These SOC values have been used as the input of the optimization algorithm to obtain the simulation results. Each curve belongs to a specific value of the SOC (the SOC values have been varied from 20% to 80% to ensure the optimal operation of the storage systems).

Figure 20 and **21** show the DC-bus voltage variations for different values of SOC for the conventional and the proposed adaptive droop controllers, respectively.

Symbols	Parameters	Values
P_o	Nominal Output Power for Battery#1 converter	500 W
P_o	Nominal Output Power for Battery#2 converter	250 W
P_o	Nominal Output Power for PV converter	500 W
f_{sw}	Switching Frequency	100 kHz
V_{nom}	Nominal DC MG Voltage	190 V DC
$V_{in_{Bat}}$	Battery Bank Voltage	80 V DC
$V_{in_{PV}}$	PV Bank Voltage	80 V DC
L_1	Battery input Inductor	$150\mu H$
L_2	PV input Inductor	$330\mu H$
C_o	Output Capacitor	$200\mu F$

Table 2.
DC/DC converter specifications in experimental.
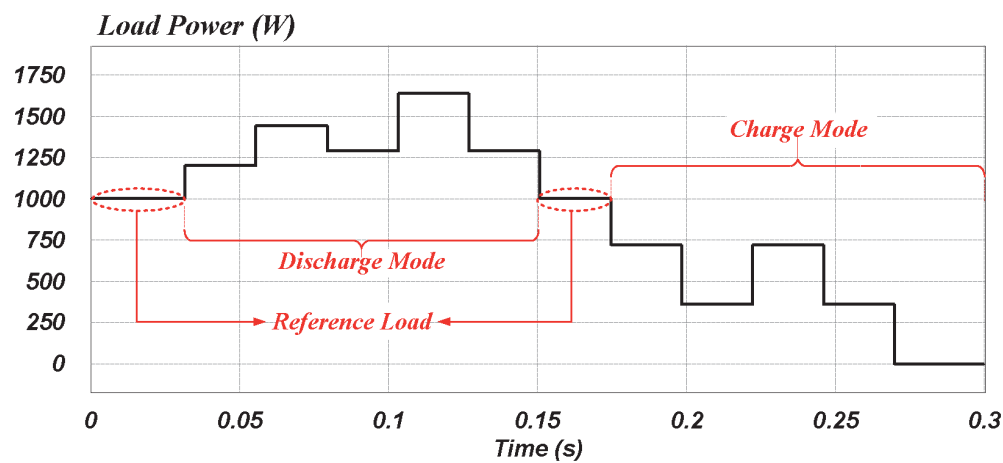
Figure 14.
Step changes (type 1) of the DC-load in DC MG.
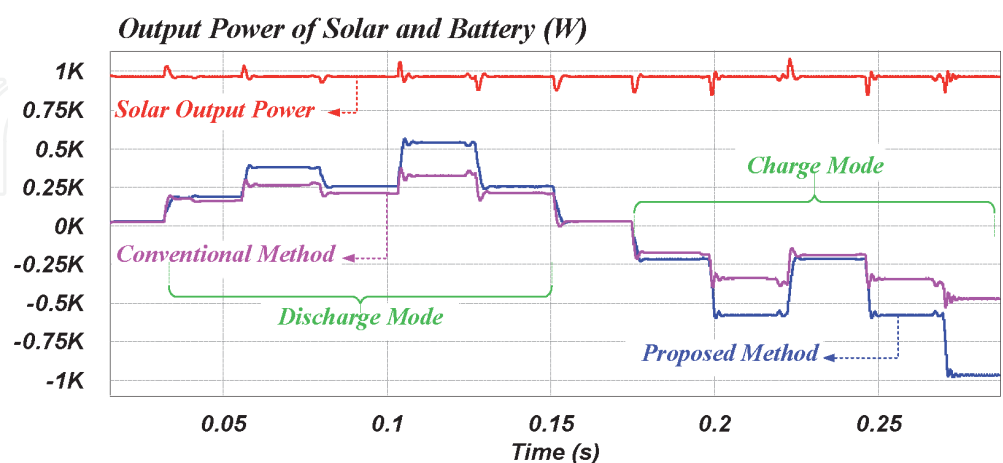
Figure 15.
Simulation result to compare the output power of the solar and battery between the proposed and conventional control method in SoC = 80%.

Figure 21 validates the superior performance of the proposed adaptive droop controller over the conventional one in regulating the DC-bus voltage for a wide range of *SOC* changes. In additions, the solar converter control system switches to the
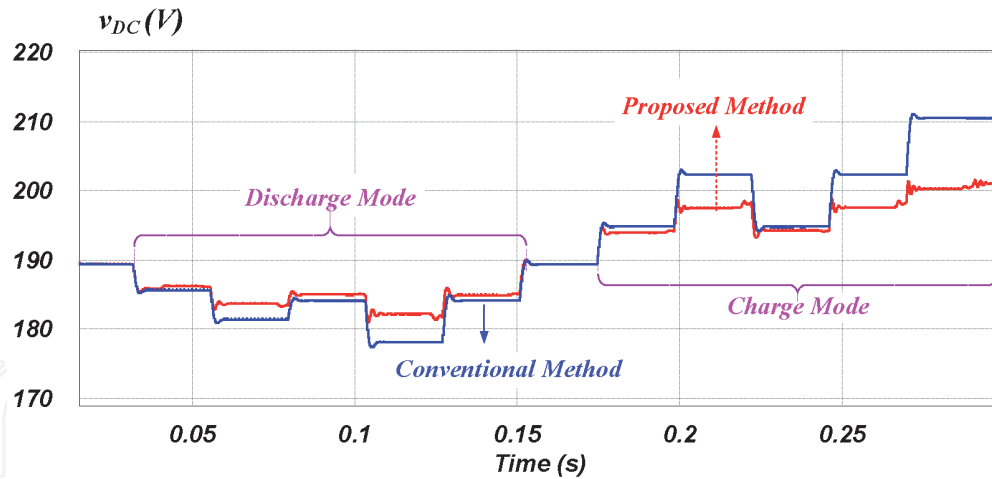
Figure 16.
Simulation result to compare the DC-bus voltage regulation in the battery between the proposed and conventional control method in SoC = 80%.
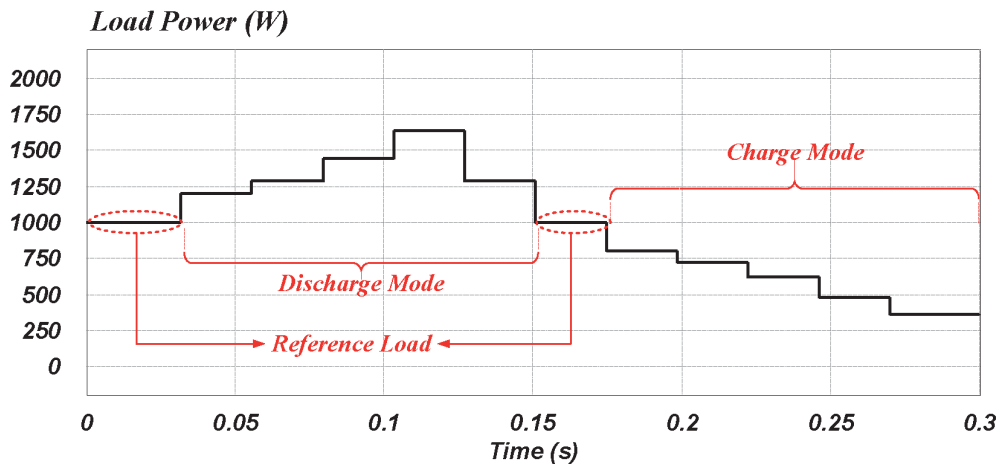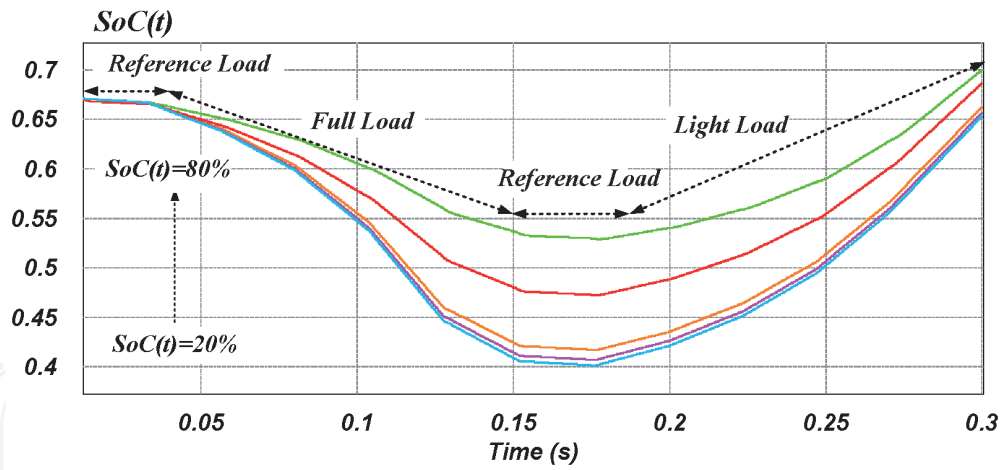

Figure 17.
*Step changes (type 2) of the DC-load in DC MG.*
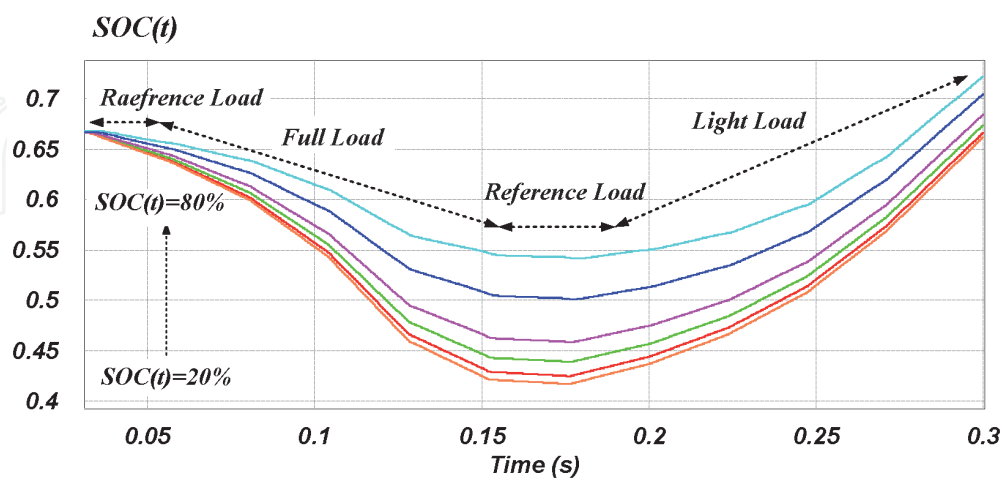
Figure 18.
Simulation results of SOC values when there are load step changes in the conventional control method.

droop control mode to fixed the DC voltage under 200 V in light load condition by state-modifier.

A small-scale DC micro-grid set-up has been implemented to evaluate the performance of the proposed method. The implemented experimental setup includes three

Figure 19.
Simulation results of SOC values for load step changes in the proposed control method.
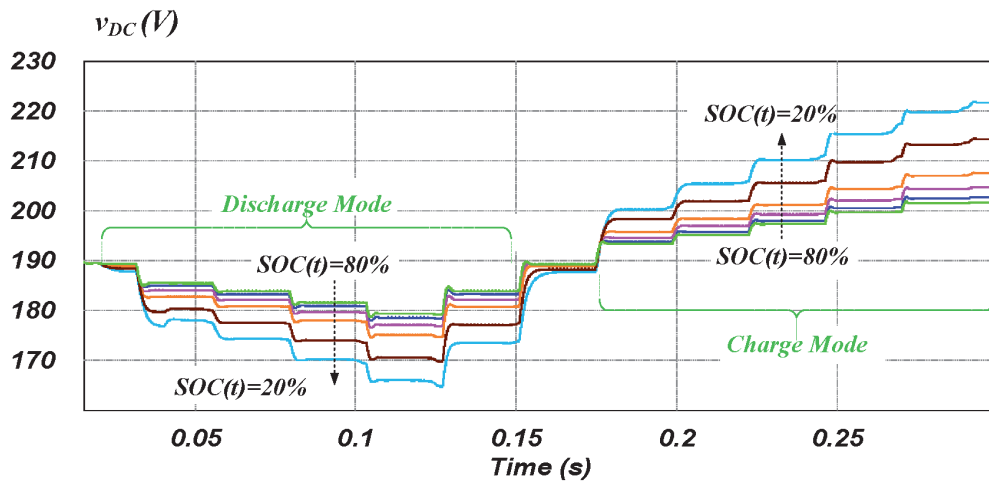
Figure 20.
Simulation result of the DC-bus voltage regulation of the battery by the load step changes in the conventional control method.
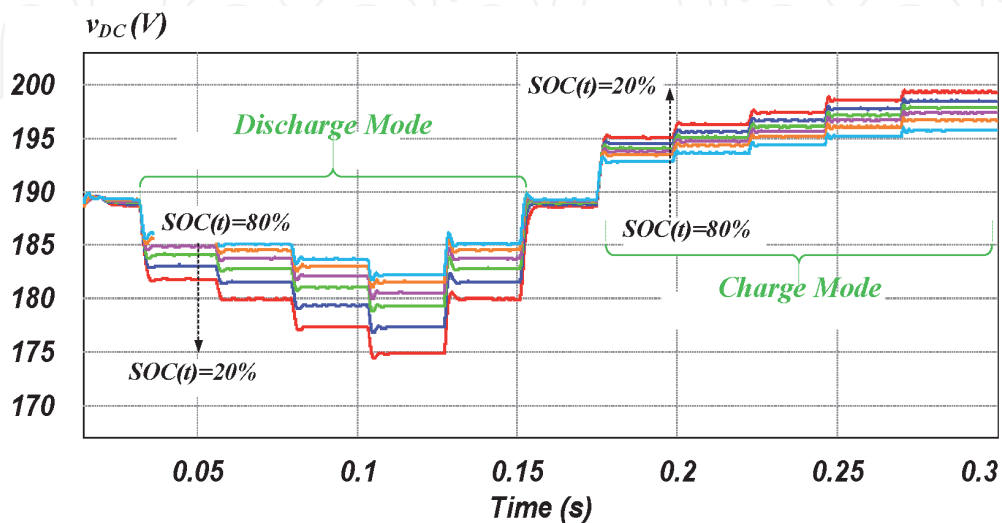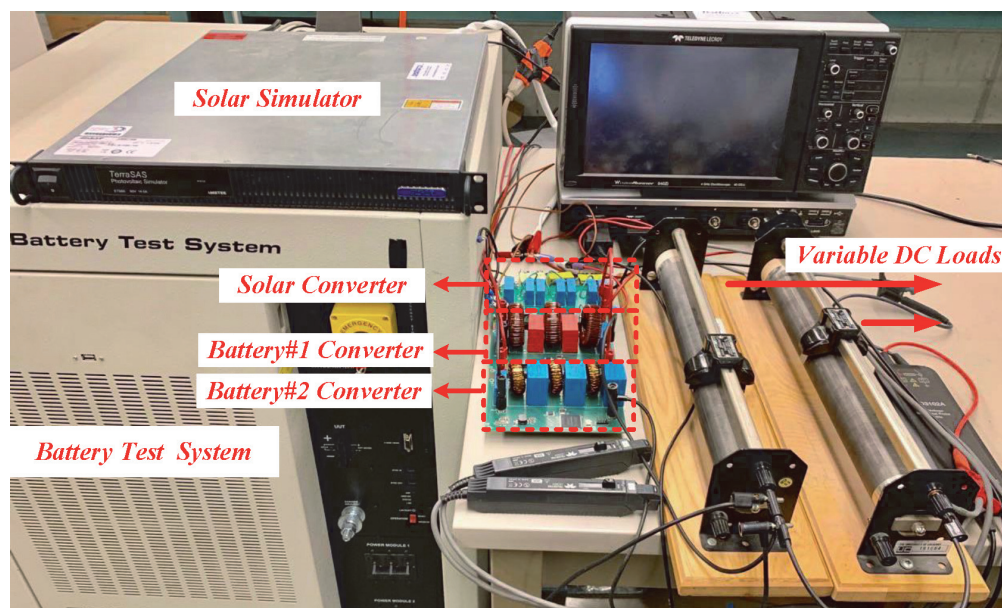

Figure 21.
DC-bus voltage regulation of the battery by the load step changes in the implemented SQP method in the proposed control method.

21
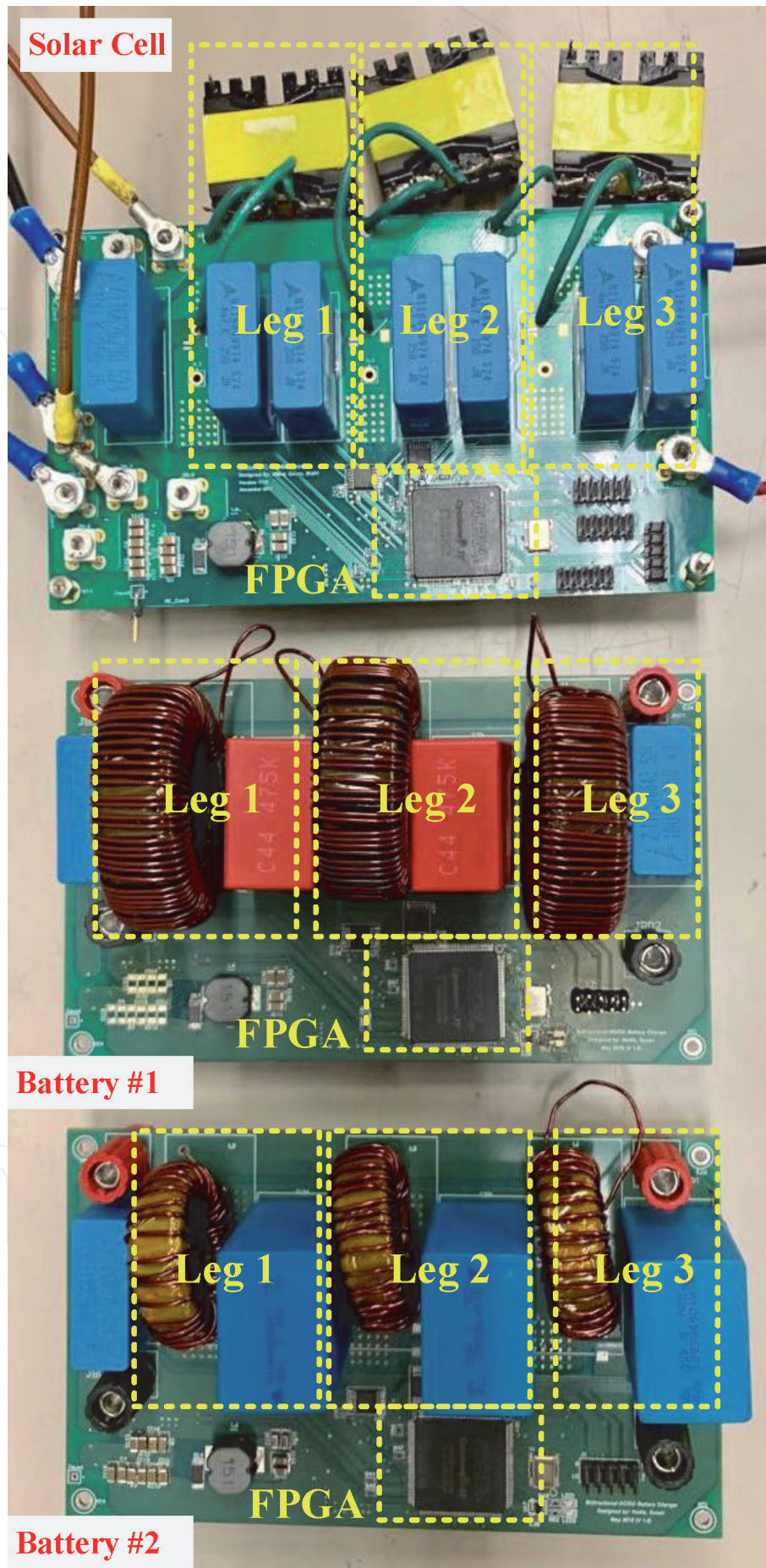
Figure 22.
Top side of the prototype DC/DC bidirectional-boost converters, the converters of the solar, battery one, and battery two.

boost converters in the power conditioning systems for the two energy storage (battery1 = 500 W and battery#1 = 250 W) and solar systems (PV panel = 500 W) with variation of DC loads. The specifications of the implemented converters are given in **Table 2**. **Figure 22** shows the experimental prototype of the bidirectional DC/DC converters, solar, battery#1, and battery#2 converters. The implemented converters use three separate phases for optimal performance (each phase changes phase 120 degrees to reduce the current wave). **Figure 23** shows a test prototype including two battery converters, a PV converter, a PV simulator, a battery simulator and a DC load to evaluate the proposed control system in the case of practical situation. For cost and safety reasons, experiments are performed at reduced power scale (1/2). All test results are based on a nominal voltage of 200V with a voltage variation of 40V. *SOC* values change from 20–80%, when load specifications change from reference load (500W) to the light load (50W) and from reference full load slow (1100W).

Figure 24 shows the high frequency wave forms of the implemented boost converter. **Figure 25** shows the performance of the PI controller in tracking the

Figure 23.
*The test bench of two batteries and PV simulator with the DC load developed in the laboratory.*
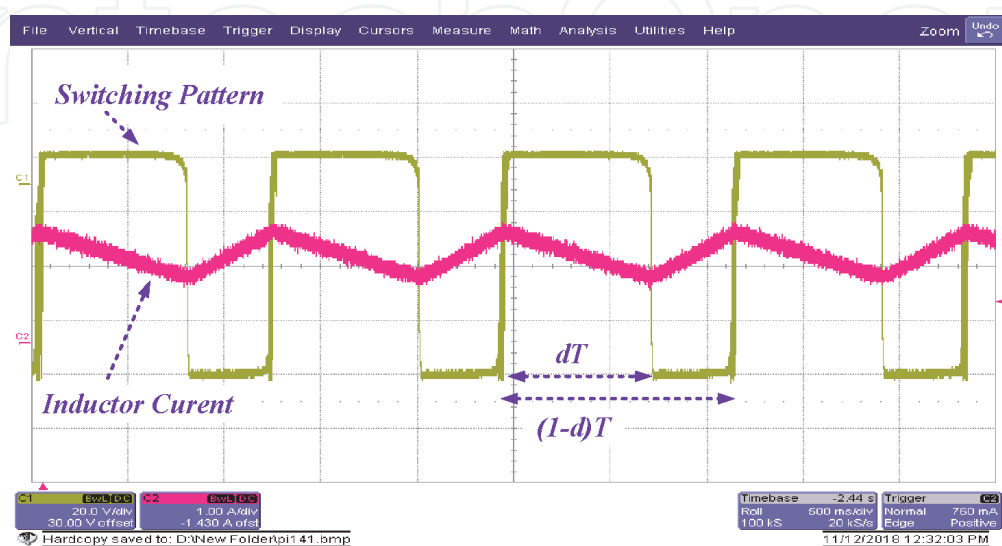
Figure 24.
Experimental result of the boost converter high frequency waveforms.

23

reference value of the output current. The proposed method is validated under light and heavy load changing conditions with $SoC = 40\%, 60\%$, and 80%. **Table 3** finalized the summary of the results obtained from the experimental setup. In **Table 3** the comparison between the proposed control system performance with the conventional droop controller performance is shown in terms of improving deviation in the DC-bus voltage as well as compensating the demanded load power. To evaluate the proposed system performance for a wide range of load variations in MG, two various cases with different step load changes considered in **Table 3**. Offering a superior performance over a wide range MG load a long with a wide range of available storage capacity (i.e, SOC of batteries) in comparison with the conventional droop is presented in **Table 3** for the proposed method. The above mentioned load changing strategies are listed as follows.

5.1 From reference to light load of $SoC = 80\%$

Figure 26 illustrates the performance of the conventional droop control when the load is changing from reference value to the light load (from 500 W to 50 W). The minimum voltage devotion in the conventional method is $17V$.
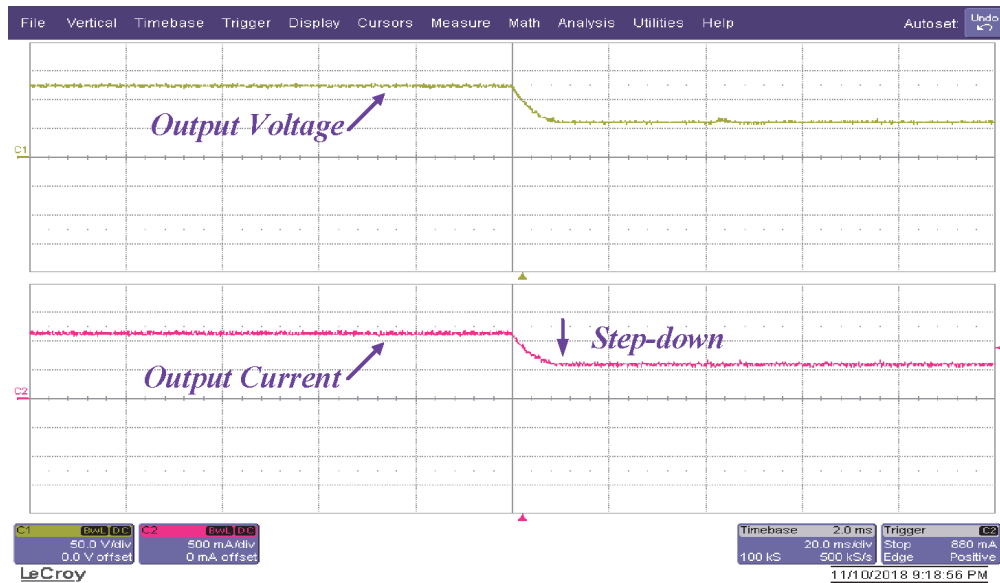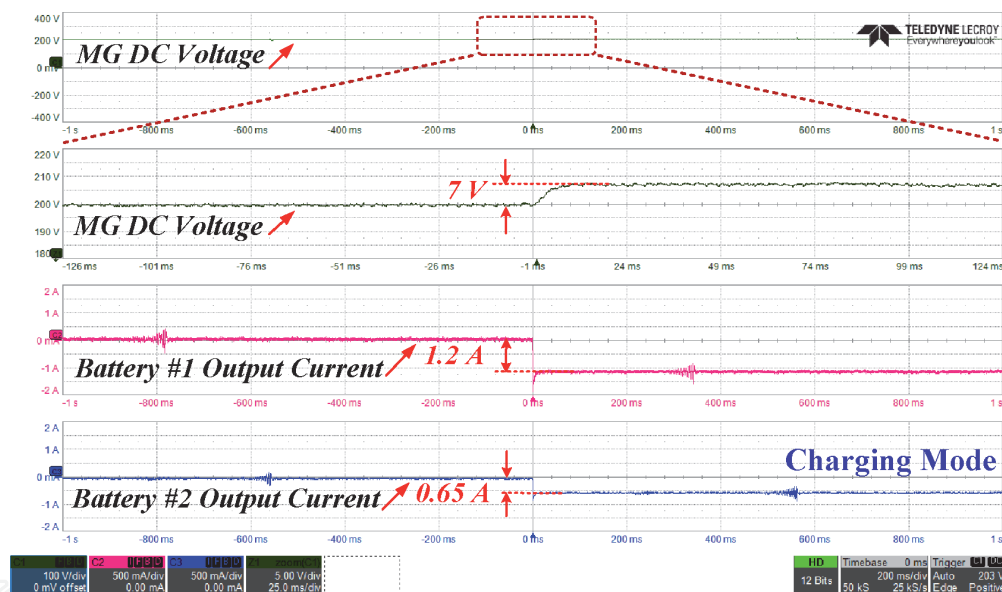

Figure 25.
Experimental result of the PI controller performance by creating a step change in the load value.

Load step change	Method	Batteries SOC value	Voltage deviation	Voltage deviation improvement*	Compensated load current	
					Battery #1	Battery #2
Reference to Light Load (500 W to 50 W)	Conventional	NA (80%)	17 V	NA (0%)	0.9A	0.42A
	Proposed	80%	7 V	58%	1.2A	0.65A
Reference to Full Load (500 W to 1100 W)	Conventional	NA (80%)	20 V	NA (0%)	1.1A	0.55A
		80%	6 V	71%	1.8A	0.93A
	Proposed	60%	11 V	45%	1.5A	0.75A
		40%	14 V	31%	1.3A	0.65A

Table 3.
Performance of the proposed control system in improving the DC-bus voltage deviation as well as compensating the load demanded power in comparison with the conventional droop controller.
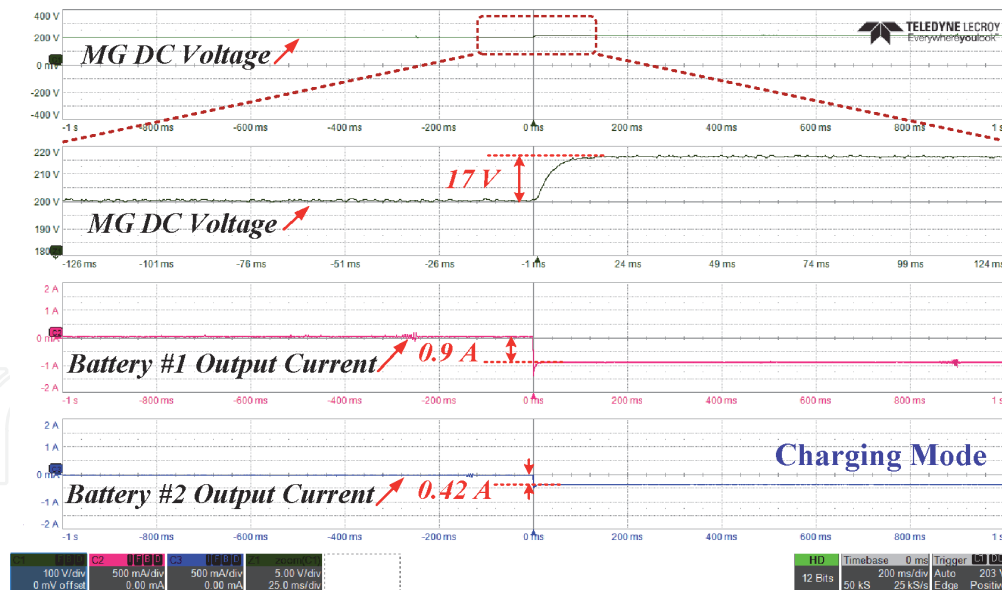
Figure 26.
Experimental result of the DC-bus voltage and batteries output current in conventional droop control method operating by one step change of load value from 500W to 50W, with SOC = 80%.
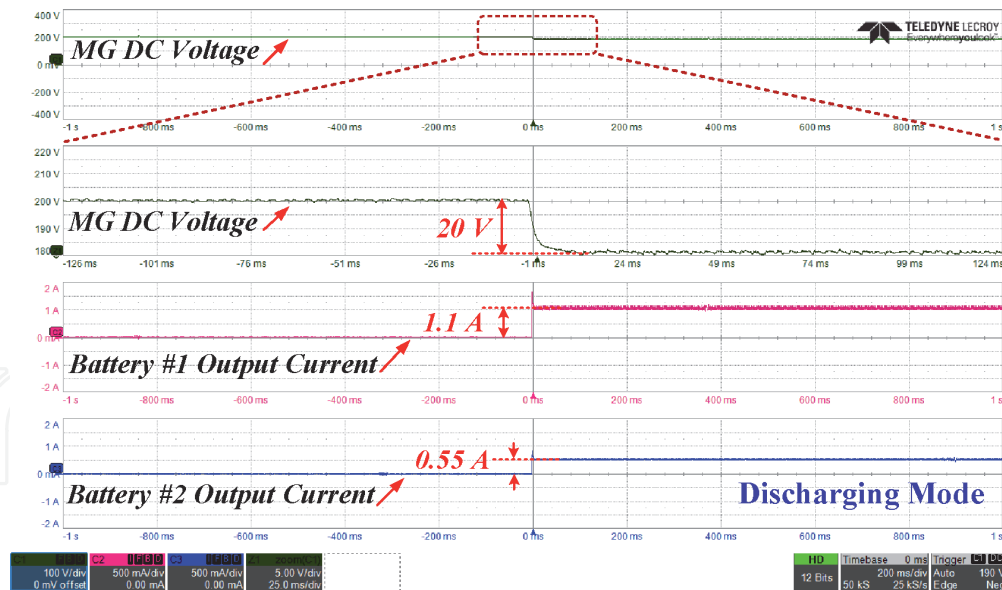

Figure 27.
Experimental result of the DC-bus voltage and batteries output current in proposed droop control method operating by one step change of load value from 500W to 50W, with SOC = 80%.
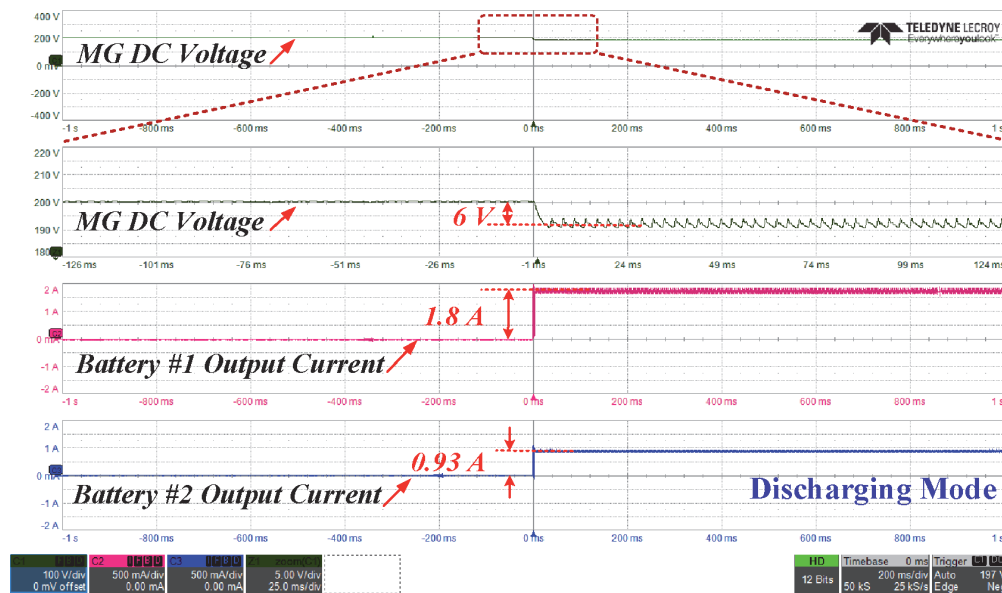
Figure 27 verifies the ability of the proposed controller in maintaining the DC-bus voltage against load steps for $SOC = 80\%$ in a lower voltage deviation, which voltage deviation is only $7V$. According to **Figure 27** and **Table 3**, the proposed controller could successfully compensate a higher percentages of load demanded power in comparison with the conventional method while offering a precise current sharing between two battery units.

5.2 From reference to full load of $SoC = 80\%$

Figure 28 presented the conventional droop control performance when the load changes from reference value to the full load (from $500W$ to $1100W$). The minimum voltage devotion in the conventional method is $6V$. **Figure 29** verifies the

Figure 28.
Experimental result of the DC-bus voltage and batteries output current in conventional droop control method operating by one step change of load value from 500W to 1100W, with SOC = 80%.
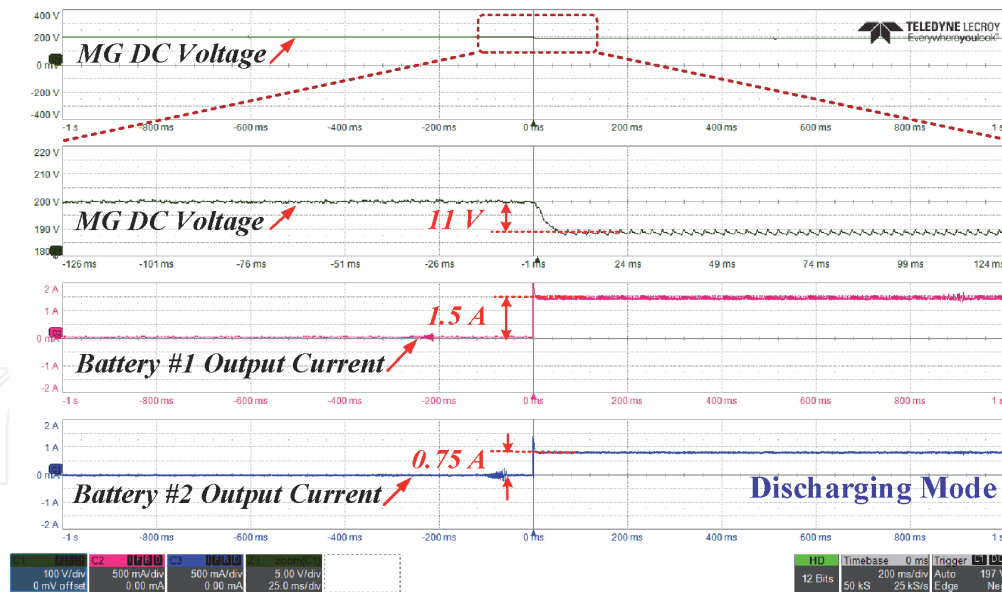

Figure 29.
Experimental result of the DC-bus voltage and batteries output current in proposed droop control method operating by one step change of load value from 500W to 1100W, with SOC = 80%.

ability of the proposed controller in maintaining the DC-bus voltage against load steps for $SOC = 80\%$ in a lower voltage deviation, which voltage deviation is only $6V$. According to **Figure 29** and **Table 3**, the proposed controller could successfully compensate a higher percentages of load demanded power in comparison with the conventional method while offering a precise current sharing between two battery units.

5.3 From reference to full load of $SoC = 80\%, 60\%,$ *and* 40%

Figures 29–31 illustrated the proposed control system performance in maintaining the DC voltage at three values of $SoC = 80\%, 60\%,$ and 40% in discharge mode. The voltage deviation in the three cases are respectfully, $6V$, $11V$, and

Figure 30.
Experimental result of the DC-bus voltage and batteries output current in proposed droop control method operating by one step change of load value from 500W to 1100W, with SOC = 60%.
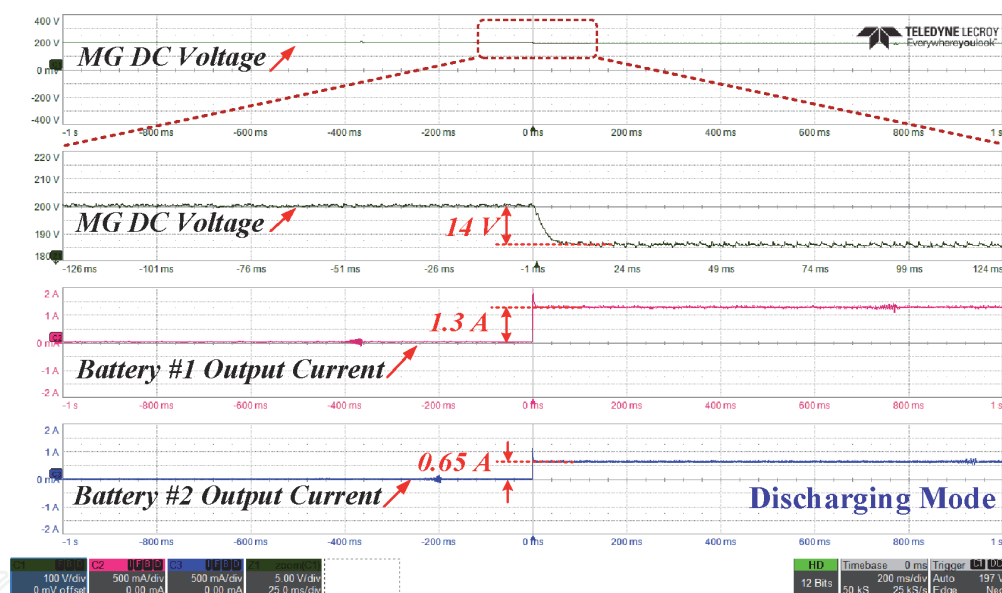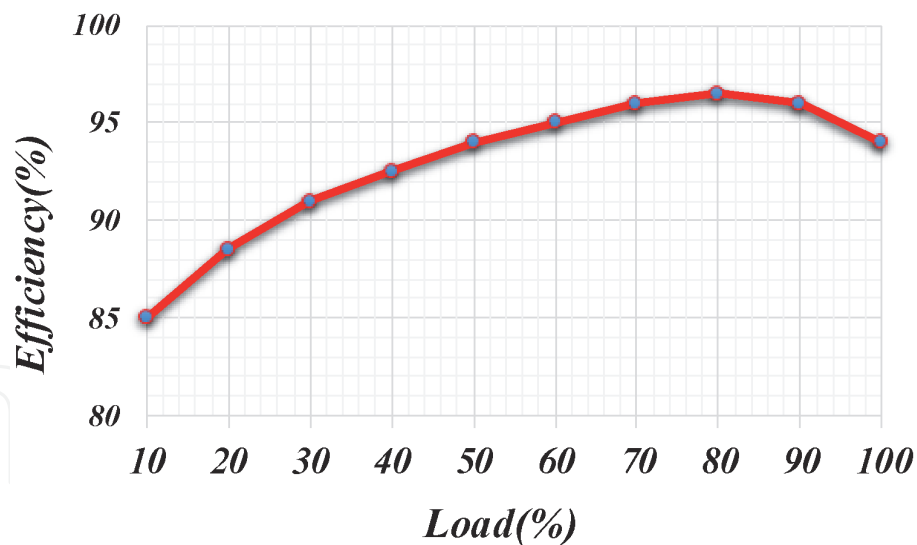

Figure 31.
Experimental result of the DC-bus voltage and batteries output current in proposed droop control method operating by one step change of load value from 500W to 1100W, with SOC = 40%.

$14V$. The results show that even in the worst case ($SoC = 40\%$) the performance of the proposed system is better than the conventional one.

Figure 32 shows the efficiency curve of the battery converter in the full range of output power variation from zero to full load. The rated power of the battery converter is 500 W as mentioned in **Table 2**. It should be mentioned that the proposed control system is a supervisory control system that control the flow of power between the converter and the DC grid by providing power references of the converter controller. Therefore, the proposed control system does not have any effect on the efficiency level of the converters and there are no extra losses caused by the proposed method. Moreover, the proposed method affects the control system only in transients and in steady-state operation, the control system is not affected by the proposed method.

Figure 32.
Efficiency curves of the DC converter when the load is changing from light to full load.

6. Conclusion

In this chapter, a new adaptive droop control technique for the Battery or ESS has been proposed in the islanded mode. The proposed method provides a very tight DC-bus voltage regulation, while charge/discharge control task of the battery system is performed. In this control scheme, two extra operation modes (i.e., fast charge and fast discharge) has been proposed, which can offer an optimal performance for the DC MG. Thus, the extra power generated by the renewable energy sources can effectively charge the battery so fast. In case of voltage dropping, the battery is fast discharged, which can keep the desired DC-bus voltage range. In addition, a nonlinear optimization method has been introduced to determine the adaptive parameters in the optimal droop controller. Experimental and simulation results have validated the superior performance of the presented controller in comparison with the conventional controller.

Author details

Hadis Hajebrahimi*, Sajjad Makhdoomi Kaviri, Suzan Eren and Alireza Bakhshai
Department of Electrical and Computer Engineering, Queen's University, Kingston, ON, Canada

*Address all correspondence to: hadis.hajebrahimi2@gmail.com

IntechOpen

References

[1] F. Blaabjerg, Zhe Chen and S. B. Kjaer, "Power electronics as efficient interface in dispersed power generation systems," in IEEE Transactions on Power Electronics, vol. 19, no. 5, pp. 1184-1194, Sept. 2004.

[2] D. E. Olivares, A. Mehrizi-Sani, A. H. Etemadi, C. A. Canizares, R. Iravani, M. Kazerani, A. H. Hajimiragha, O. Gomis-Bellmunt, M. Saeedifard, R. Palma-Behnke, and N. D. Hatziargyriou, "Trends in Microgrid control," IEEE Transactions on Smart Grid, vol. 5, no. 4, pp. 1905–1919, Jul.

[3] J. M. Guerrero, M. Chandorkar, T. L. Lee and P. C. Loh, "Advanced Control Architectures for Intelligent Microgrids—Part I: Decentralized and Hierarchical Control," in IEEE Transactions on Industrial Electronics, vol. 60, no. 4, pp. 1254-1262, April 2013.

[4] J. M. Guerrero, J. C. Vasquez, J. Matas, L. G. de Vicuna and M. Castilla, "Hierarchical Control of Droop-Controlled AC and DC Microgrids—A General Approach Toward Standardization," in IEEE Transactions on Industrial Electronics, vol. 58, no. 1, pp. 158-172, Jan. 2011.

[5] H. Han, X. Hou, J. Yang, J. Wu, M. Su and J. M. Guerrero, "Review of Power Sharing Control Strategies for Islanding Operation of AC Microgrids," in IEEE Transactions on Smart Grid, vol. 7, no. 1, pp. 200-215, Jan. 2016.

[6] Y. Han, H. Li, P. Shen, E. A. A. Coelho and J. M. Guerrero, "Review of Active and Reactive Power Sharing Strategies in Hierarchical Controlled Microgrids," in IEEE Transactions on Power Electronics, vol. 32, no. 3, pp. 2427-2451, March 2017.

[7] F. Wang, Y. Pei, D. Boroyevich, R. Burgos, and K. Ngo, "Ac vs. Dc Distribution for Off-Shore Power Delivery," in 34th Annual Conference of IEEE Industrial Electronics (IECON), 2018, pp. 2113–2118.

[8] J. Park and J. Candelaria, "Fault Detection and Isolation in Low-Voltage DC-Bus Microgrid System," in IEEE Transactions on Power Delivery, vol. 28, no. 2, pp. 779-787, April 2013.

[9] L. Meng, Q. Shafiee, G. Ferrari Trecate, H. Karimi, D. Fulwani, X. Lu, and J. M. Guerrero, "Review on Control of DC Microgrids, â" IEEE J. Emerg. Sel. Top. Power Electron., pp. 1–1, 2017.

[10] E. Rodriguez-diaz, J. C. Vasquez, and J. M. Guerrero, "Intelligent DC homes in future sustainable energy systems: When efficiency and intelligence work together," IEEE Consum. Electron. Mag., vol. 5, no. 1, pp. 74–80, 2016.

[11] A. Khorsandi, M. Ashourloo, and H. Mokhtari, "A decentralized control method for a low-voltage DC microgrid," IEEE Trans. Energy Convers.vol. 29, no. 4, pp. 793–801, Dec. 2014.

[12] Y. Han, H. Li, P. Shen, E. A. A. Coelho and J. M. Guerrero, "Review of Active and Reactive Power Sharing Strategies in Hierarchical Controlled Microgrids," in IEEE Transactions on Power Electronics, vol. 32, no. 3, pp. 2427-2451, March 2017.

[13] Y. Gu, X. Xiang, W. Li and X. He, "Mode-Adaptive Decentralized Control for Renewable DC Microgrid with Enhanced Reliability and Flexibility," in IEEE Transactions on Power Electronics, vol. 29, no. 9, pp. 5072-5080, Sept. 2014.

[14] S. Augustine, M. K. Mishra, and N. Lakshminarasamma, "Adaptive droop control strategy for load sharing and circulating current minimization in low-

voltage standalone DC microgrid," IEEE Trans. Sustain. Energy, vol. 6, no. 1, pp. 132–141, Jan. 2015.

[15] T. Dragicevic et al., "DC Microgrids; Part I: A Review of Control Strategies and Stabilization Techniques,"IEEE Trans. Power Electron., vol. 31, no. 7, July 2016, pp. 4876–4891.

[16] F. Chen, R. Burgos, D. Boroyevich, J. C. Vasquez and J. M. Guerrero, "Investigation of Nonlinear Droop Control in DC Power Distribution Systems: Load Sharing, Voltage Regulation, Efficiency, and Stability," in IEEE Transactions on Power Electronics, vol. 34, no. 10, pp. 9404-9421, Oct. 2019.

[17] P. Prabhakaran, Y. Goyal and V. Agarwal, "Novel Nonlinear Droop Control Techniques to Overcome the Load Sharing and Voltage Regulation Issues in DC Microgrid," in IEEE Transactions on Power Electronics, vol. 33, no. 5, pp. 4477-4487, May 2018.

[18] Chen, D and Xu, L 2017, 'AC and DC microgrid with distributed energy resources' in Technologies and Applications for Smart Charging of Electric and Plug-in Hybrid Vehicles. Springer, pp. 39-64., 10.1007/978-3-319-43651-7-2.

[19] X. Lu, K. Sun, J. M. Guerrero, J. C. Vasquez, and L. Huang, "State-of-charge balance using adaptive droop control for distributed energy storage systems in DC microgrid applications," IEEE Trans. Ind. Electron., vol. 61, no. 6, pp. 2804–2815, Jun. 2014.

[20] Dragicevic, T., Lu, X., Vasquez, J., et al.: 'DC microgrids – part II: a review of power architectures, applications, and standardization issues', IEEE Trans. Power Electron., 2016, 31, (5), pp. 3528–3549.

[21] Mahmood, H., Michaelson, D., Jiang, J.: 'Decentralized power management of a PV/battery hybrid unit in a droop controlled islanded microgrid', IEEE Trans. Power Electron., 2015, 30, (12), pp. 7215–7229

[22] J. M. Guerrero, J. C. Vasquez, J. Matas, L. G. de Vicuna, and M. Castilla, "Hierarchical control of droop-controlled AC and DC microgrids—A general approach toward standardization," IEEE Trans. Ind. Electron., vol. 58, no. 1, pp. 158–172, Jan. 2011.

[23] IEEE 929–2000 Standard, "IEEE Recommended Practice for Utility Interface of Photovoltaic (PV) Systems", April 2000.

[24] A. Kwasinski, "Quantitative evaluation of DC microgrids availability: Effects of system architecture and converter topology design choices," IEEE Trans. Power Electron., vol. 26, no. 3, pp. 835–851, Mar. 2011.

[25] D. Jovcic, M. Taherbaneh, J. Taisne, and S. Nguefeu, "Offshore DC grids as an interconnection of radial systems: protection and control aspects," IEEE Trans. Smart Grid, vol. 6, no. 2, pp. 903–910, 2015.

[26] J. Park and J. Candelaria, "Fault Detection and Isolation in Low-Voltage DC-Bus Microgrid System,"in IEEE Transactions on Power Delivery, vol. 28, no. 2, pp. 779-787, April 2013.

[27] Q. Shafiee, J. M. Guerrero and J. C. Vasquez, "Distributed Secondary Control for Islanded Microgrids - A Novel Approach," in IEEE Transactions on Power Electronics, vol. 29, no. 2, pp. 1018-1031, Feb. 2014.

[28] E. Barklund, N. Pogaku, M. Prodanovic, C. Hernandez-Aramburo and T. C. Green, "Energy Management in Autonomous Microgrid Using Stability-Constrained Droop Control of Inverters," in IEEE Transactions on Power Electronics, vol. 23, no. 5, pp. 2346-2352, Sept. 2008

[29] Y. Karimi, H. Oraee, M. S. Golsorkhi and J. M. Guerrero, "Decentralized Method for Load Sharing and Power Management in a PV/Battery Hybrid Source Islanded Microgrid," in IEEE Transactions on Power Electronics, vol. 32, no. 5, pp. 3525-3535, May 2017.

[30] E. Barklund, N. Pogaku, M. Prodanovic, C. Hernandez-Aramburo and T. C. Green, "Energy Management in Autonomous Microgrid Using Stability-Constrained Droop Control of Inverters," in IEEE Transactions on Power Electronics, vol. 23, no. 5, pp. 2346-2352, Sept. 2008

[31] N. L. Diaz, T. Dragičević, J. C. Vasquez, and J. M. Guerrero, "Intelligent distributed generation and storage units for DC microgrids—A new concept on cooperative control without communications beyond droop control," IEEE Trans. Smart Grid, vol. 5, no. 5, pp. 2476–2485, Sep. 2014.

[32] Y. Gu, X. Xiang, W. Li, and X. He, "Mode-adaptive decentralized control for renewable DC microgrid with enhanced reliability and flexibility," IEEE Trans. Power Electron., vol. 29, no. 9, pp. 5072–5080, Sep. 2014.

[33] E. M. L. Beale, Numerical Methods6in: Nonlinear Programming, J. Abadie, ed., NorthHolland, Amsterdam, 1967.

[34] Powell, M. J. D. "A Fast Algorithm for Non-linearly Constrained Optimization Calculations." Numerical Analysis, ed. G. A. Watson, Lecture Notes in Mathematics, Springer-Verlag, Vol. 630, 1978

[35] K. Wu, C. W. de Silva and W. G. Dunford, "Stability Analysis of Isolated Bidirectional Dual Active Full-Bridge DC–DC Converter With Triple Phase-Shift Control," in IEEE Transactions on Power Electronics, vol. 27, no. 4, pp. 2007-2017, April 2012.